Development of a Hydraulic Energy Storage System for Hybrid Wind Turbine Transmissions

A THESIS

SUBMITTED TO THE FACULTY OF THE GRADUATE SCHOOL

OF THE UNIVERSITY OF MINNESOTA

BY

Eric Benjamin Mohr

IN PARTIAL FULFILLMENT OF THE REQUIREMENTS

FOR THE DEGREE OF

MASTER OF SCIENCE

Professor Kim Stelson

May, 2021

Acknowledgements

I would like to sincerely express my gratitude to all that have helped me through completing this thesis. I would first like to thank Professor Kim Stelson for being an excellent mentor and guide during this project. Without his support this project would not have happened.

I would also like to thank the professors on my thesis committee, Professor Jim Van de Ven and Professor Paul Imbertson. Thank you for taking the time to be on my committee, and thank you both for your expertise in accumulators and wind energy, respectively. I would like to thank professor Perry Li for his input into this project and his expertise and educational advice.

I would like to thanks James Amelung from Hagglunds, Russ Luzinski from Linde, and Aaron Yoder from Bonfiglioli for their contributions and input to the project. These experts have collectively improved my knowledge tenfold.

I would like to thank Dr. Biswaranjan Mohanty for his contributions to this project, for his research advice and leadership, and for being a good friend. His previous work in

developing the power regenerative test stand and his expertise in hydraulics and controls were essential to completion of this project.

I would like to thank Ph.D student Daniel Escobar Naranjo for his dedication to this project and progressing the research of our group. He has provided support and guidance on many occasions, and has some bright ideas for future work.

I wish to extend my thanks to undergraduate researches Debbie Ajagbe and Neil Garcia for their significant contributions to this project. Debbie for her significant impact in researching the accumulator heat transfer model, and Neil for his significant contribution is design and construction of the test platform.

I would like to extend my thanks to the rest of professor Stelson's group during my tenure for their positive impact on this research.

I would like to thank the University of Minnesota and the Department of Mechanical Engineering for the opportunity to complete this research. I would also like to thank Richard Maharaj for the significant amount of time he has invested into helping with the hybrid project construction.

Lastly, but perhaps most importantly I would like to personally thank my family and long-time girlfriend Kenzie for their never ending support. In the hardest of times they were always there for support and guidance.

Dedication

I dedicate this thesis to the pursuit of knowledge.

Abstract

Mid-size wind turbines are an under-recognized means to help prevent irreversible climate damage caused by unprecedented human-made carbon emissions. A high-power hydraulic energy storage system can be added to turbine transmissions to capture energy in high wind speeds, and release energy in low wind speeds. The hybrid system stabilizes the output power of the transmission, and increases reliability while offering ancillary benefits such as fault-ride through and pitch and yaw control in severe weather. The hybrid system was constructed. Experimental characterization of hybrid parameters determined that a modified heat transfer model of the accumulator is realistic, and that the thermal time constant of the accumulator is around 80 seconds. A high fidelity simulation is produced which is experimentally validated. The simulation is then used to find the additional annual energy production compared to the non-hybrid system is 3.5%. This value can only be attained with the addition of a clutch and directional valve.

Contents

Acknowledgements **i**

Dedication **iii**

Abstract **iv**

List of Tables **ix**

List of Figures **x**

1 Introduction **1**

1.1 Global Climate Crisis 1

1.2 Renewable Energy Path 3

1.3 Utility Wind 4

1.4 Distributed Wind 5

1.5 Conventional and Hydrostatic Mid-size Turbines 6

1.6 Conventional Wind Turbine Operation 8

1.7 Hybrid System 9
1.8 Research Objective 12
1.8.1 Key Contributions 13
1.9 Chapter Overview 13

2 Hybrid System Design, Modelling, Control, and Preliminary Simulation 14

2.1 Hybrid System Architecture 14
2.2 Dynamic Modeling 16
2.2.1 Rotor Dynamics 16
2.2.2 Pressure Dynamics 17
2.2.3 Accumulator Dynamics 17
2.3 Accumulator Modeling 18
2.3.1 Adiabatic and Isothermal 18
2.3.2 Heat Transfer Method 20
2.4 Control 21
2.4.1 HST Turbine Standard Control 22
2.4.2 Hybrid System Control 22
2.4.3 Controller Mode V 25
2.5 Preliminary Simulation 27

3 Hardware Modification 31

3.1 HST Test Stand 31
3.2 Hybrid Test Platform 33
3.2.1 Accumulator 34
3.2.2 Secondary Pump 36
3.2.3 Gearbox 37
3.2.4 Clutch 37
3.3 ESS Design 38
3.4 Instrumentation 39

4 Experimental Results **40**

4.1 ESS Loss Characterization 41
4.2 Accumulator Experiments 44
4.2.1 Characterizing Accumulator Model Constants 44
4.2.2 Characterization of Accumulator 46
4.2.3 Accumulator Losses to Pump Cooling 51
4.3 Step Wind 54
4.4 Turbulent Wind 59
4.5 Annual Energy Production 62

5 Conclusions and Future Work **68**

5.1 Conclusion 68
5.2 Future Research 70

5.2.1 Improving Control Strategies 70
5.2.2 Advanced Control Strategies 70
5.2.3 Detailed Cost Analysis 71
5.2.4 Pitch and Yaw Control 71
5.2.5 Holistic Hydraulic System 72

References **73**

Appendix A. Controller Stability Validation **79**

Appendix B. Gearbox Torque Limiting Control **83**

Appendix C. ESS Shaft Design **85**

Appendix D. Special Component Designs **87**

Appendix E. Mounting Plate FEA **91**

Appendix F. Hydraulic Circuit **93**

Appendix G. Potential Concerns **95**

Appendix H. Driver **100**

Appendix I. Instrumentation and Uncertainty **102**

I.1 Sensors 102
I.2 Uncertainty 103

List of Tables

2.1 Rule Based Control 25

2.2 Mode V 26

2.3 Turbine and Simulation Parameters 27

3.1 Sensors 39

4.1 Seconds to Charge/Discharge 50

4.2 Discharging rates at centered swash plate 52

4.3 Quantifying accumulator losses 53

4.4 Accumulator Losses in Simulation 53

4.5 Operating Cases of Losses in Simulation 64

4.6 Percent of Additional Annual Energy Produced 65

List of Figures

1.1 Annual Global Carbon Emissions 2

1.2 Global Temperature Increase with Different Human Intervention Levels 3

1.3 Renewable Energy Trend 4

1.4 HST Wind Turbine Schematic 7

1.5 Wind Turbine Regions of Operation 8

1.6 Wind Spectrum 9

1.7 Hybrid System Storage Goal 10

2.1 Hybrid System Architecture 15

2.2 Preliminary Simulation Results 28

3.1 Power Regenerative HST Test Platform 32

3.2 Upgraded Power Regenerative HST Test Platform 33

3.3 Accumulator Sizing 35

3.4 Secondary Pump Modes of Operation 36

4.1 HSD Power 41

4.2 HST System 42
4.3 Hybrid System with Zero Displacement 43
4.4 Characterization of Accumulator Model Constants 45
4.5 Characterization of Accumulator 47
4.6 Charging and Discharging of the Accumulator 50
4.7 Step Wind Results 55
4.8 Step Wind Results with Non-Hybrid System 57
4.9 Turbulent Wind Results 60
4.10 Rayleigh Wind Speed Distribution for IEC Class II Wind 63
A.1 Root Locus of Problematic Transfer Function 80
A.2 Response of System with Negative Gain 81
B.1 Gearbox Torque vs Wind Speed 84
C.1 HST Platform Low Speed Shaft - Before 85
C.2 Energy Storage System Shaft 86
D.1 Designed Mounting Plates 88
D.2 Cut view of adapter 89
D.3 Torque Sensor Mount 90
E.1 Designed Mounting Plates FEA 92
F.1 Hydraulic Schematic 94
G.1 Minimum Allowable Suction Pressure 96
G.2 Secondary Pump Diagram 97

G.3 System Relief Valve 98

H.1 Driver Signal 101

I.1 Activa Sensor Array 103

I.2 Futek TRS 605 104

Chapter 1

Introduction

1.1 Global Climate Crisis

The Earth is undergoing unprecedented climate change. The effects of atmospheric greenhouse gasses such as $C0_2$ and water vapor on the temperature of the planet has been documented as early as 1896, and coal burning has been shown to produce these greenhouse gasses since the late 1890s [1]. A warning about the negative effects of fossil fuel burning on the climate were not published until 1965 [2]. Since then, fossil fuel use has increased over time, and $C0_2$ emissions are at an all time high. Figure 1.1 shows the global carbon emissions over the last century [3].

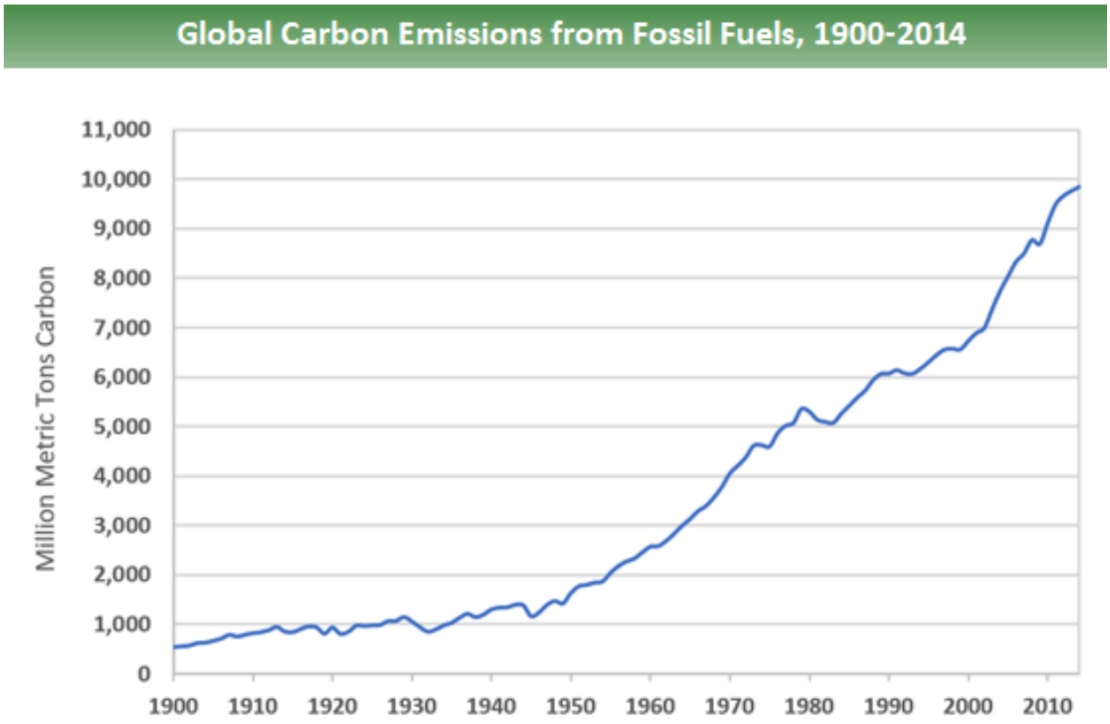

Figure 1.1: Annual Global Carbon Emissions

This increasing trend is concerning. Scientists predict the effects of climate change will include higher temperatures, an increase in droughts and heat waves, more severe weather, shrinking of the arctic, and the rising of sea levels [4].

In recent years, more access to emissions data has enabled people to take notice and push for climate activism. In 2018 the Intergovernmental Panel on Climate Change (IPCC) presented a special report which sets a goal to limit increasing global temperatures to a maximum of 1.5° C, and discusses the repercussions on the global climate [5]. Currently, the earth is on track to exceed this limit. Figure 1.2 shows the likelihood that the temperature limit will be exceeded with different levels of human intervention

[5].

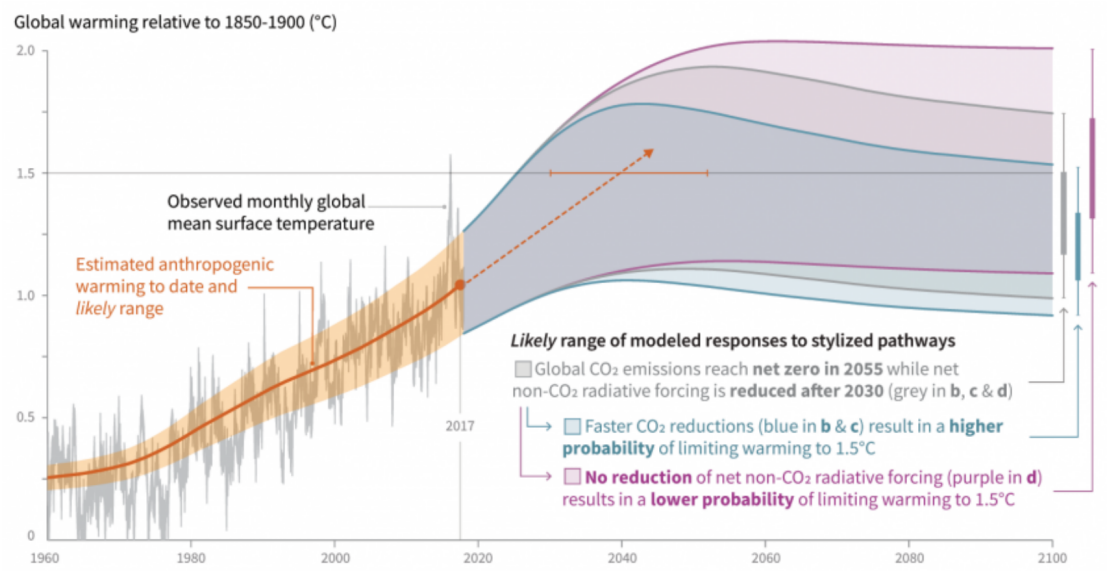

Figure 1.2: Global Temperature Increase with Different Human Intervention Levels

Efforts to reduce greenhouse gas emissions are required to reach the 1.5% goal. Renewable energy solutions are needed.

1.2 Renewable Energy Path

Renewable energies, such as wind turbines, solar panels, and wave-power generators are leading the way towards removing human dependency on carbon emitting sources of energy generation. The Paris Agreement in 2015 is a global goal to reduce carbon emissions by implementing more renewable energy sources [6]. The Paris agreement and other renewable energy incentive programs has caused the popularity of renewable energy sources to increase with time, and these sources are projected to continue to

grow, as shown in Figure 1.3 [7].

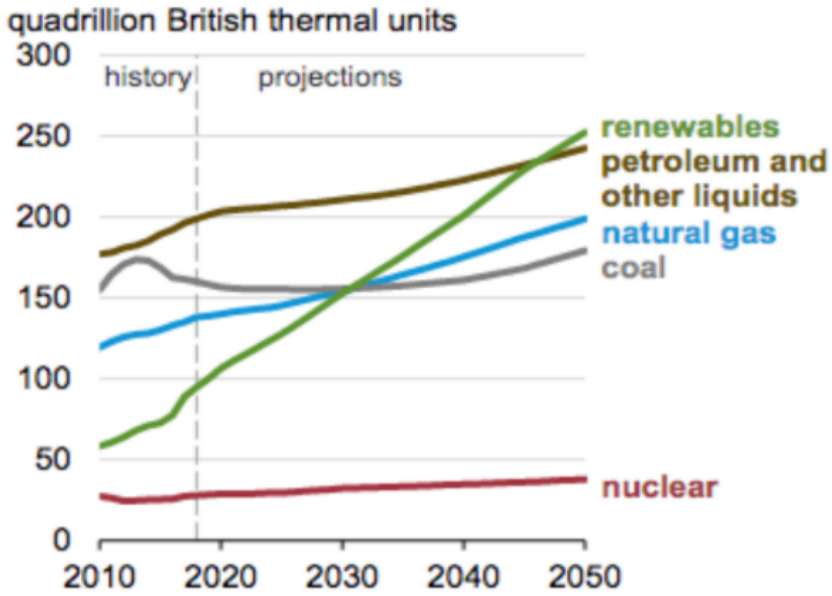

Figure 1.3: Renewable Energy Trend

Wind energy is the fastest growing source of new energy generation, and is expected to increase due to government policies, such as the United States Department Of Energy's goal to produce 20% of US energy by 2030 [8]. Most of the new wind energy research is targeted at large-scale, utility wind turbines and offshore wind farms.

1.3 Utility Wind

The majority of research and development on wind technology is occurring at the utility scale, with turbines larger than 1 MW. Large wind turbines are often investigated because they offer a high amount of power generation. Large turbines are less affected by

the earth's atmospheric boundary layer, and off-shore turbines are exposed to generally higher wind speeds [9].

Although utility scale wind is a promising revolution in renewable energies, large turbines alone cannot meet wind energy goals. Wind farms and large turbines provide large amounts of power in a single area of the electric grid. Power must be transmitted in long distance and often wasteful transmission lines, and require significant infrastructure costs [10].

A necessary part of the transition to renewable energies is utilizing all of the available resources. An important step that can be implemented quickly is the use of distributed wind.

1.4 Distributed Wind

Distributed wind refers to the vast array of individual small-scale wind turbines that supply the distributed power grid. The distributed power grid is the part of the electric grid that connects local and rural areas. Smaller sources of power generation and consumption such as rural energy cooperatives, large factories, casinos, and other local niches are connected to the distributed part of the grid. These niches can be powered with small to mid-size wind turbines.

Having more power generating sources in a distributed grid benefits the stability of the grid and creates higher quality electricity for rural areas [11]. Mid-sized wind turbines can satisfy the local power requirements while maintaining a stable grid, and

require minimal to zero infrastructure upgrades, which can cost millions [10]. These mid-sized turbines can be implemented in the short term to reach wind power goals with a lower start-up cost than utility scale turbines. Mid-sized turbines are an underrecognized market and have potential for improvement.

1.5 Conventional and Hydrostatic Mid-size Turbines

Conventional mid-size wind turbines use a large planetary gearbox to transmit power from the rotor shaft to the generator shaft.These gearboxes are fixed-ratio and require costly power electronics to convert the electricity produced to the grid frequency. The fixed-ratio gearbox transmission has poor reliability due to shock loading from the wind [12].

Meanwhile, a HydroStatic Transmission (HST) is a hydraulic-based transmission that uses a hydraulic pump and hydraulic motor, connected with a fluid coupling. This is a continuously variable transmission that allows the high-speed shaft and low-speed shaft to run at independent speeds. The low-speed shaft is connected to the rotor, and the high-speed shaft is connected to the generator. The generator shaft can be controlled to run at the grid frequency without the need for power electronics. A schematic of the HST turbine transmission is shown in Figure 1.4

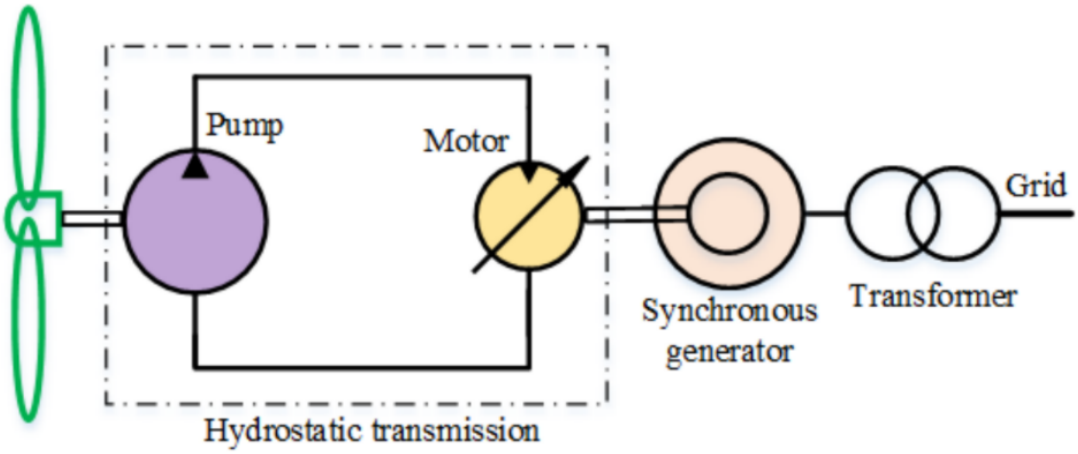

Figure 1.4: HST Wind Turbine Schematic

HST's have many practical applications outside of wind turbines. A speed-down HST is commonly used in off-road agricultural vehicles to convert a high-speed engine shaft to a high-torque drive shaft. Speed-down HST's are commonly used in agriculture and construction machines and vehicles, such as combines, tractors, and wheel loaders because of their high power density and compact and flexible housing.

In a wind turbine, a high torque rotor shaft is used to rotate a high speed generator. A speed-up HST is an ideal candidate for wind turbine transmissions because of the low weight, high reliability, resistance to shock loading, and low cost [13] [14].

HST based wind turbines are a start to improve the quality of mid-size wind turbines, but more improvements can be made. By understanding the standard operation of a turbine, potential areas for improvement are discovered.

1.6 Conventional Wind Turbine Operation

Wind turbines have four distinct regions of operation, as shown in figure 1.5. In region 1, the wind speed is too low for the turbine to generate any energy. In region 2, the wind speeds are higher than the cut-in speed, but lower than the rated wind speed. The turbine is controlled to maximize the amount of power captured. In region 3, the wind speed is above the rated wind speed and below the cut-out speed. Turbine blades are pitched to intentionally limit the amount of power taken on by the turbine [15]. This is done to prevent damage to the turbine transmission. In region 4, the wind speed is too high and can potentially cause catastrophic failure. The turbine is intentionally braked to prevent damage.

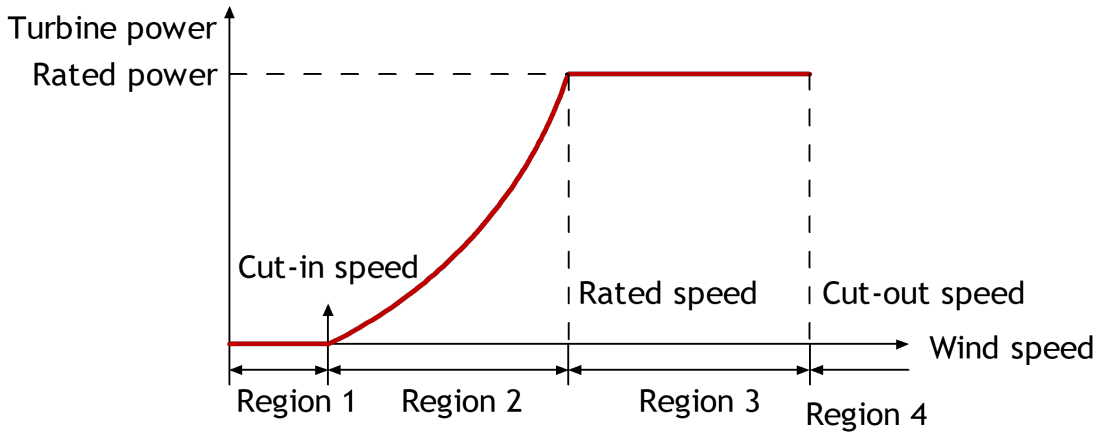

Figure 1.5: Wind Turbine Regions of Operation

The blade pitch control strategy in region 3 is slow. The average blade can pitch at a speed of 1 degree per 10 seconds [16]. Meanwhile, the wind speed changes at a faster pace.

Figure 1.6 is a popularized wind distribution that shows the common frequencies of wind variation [17].

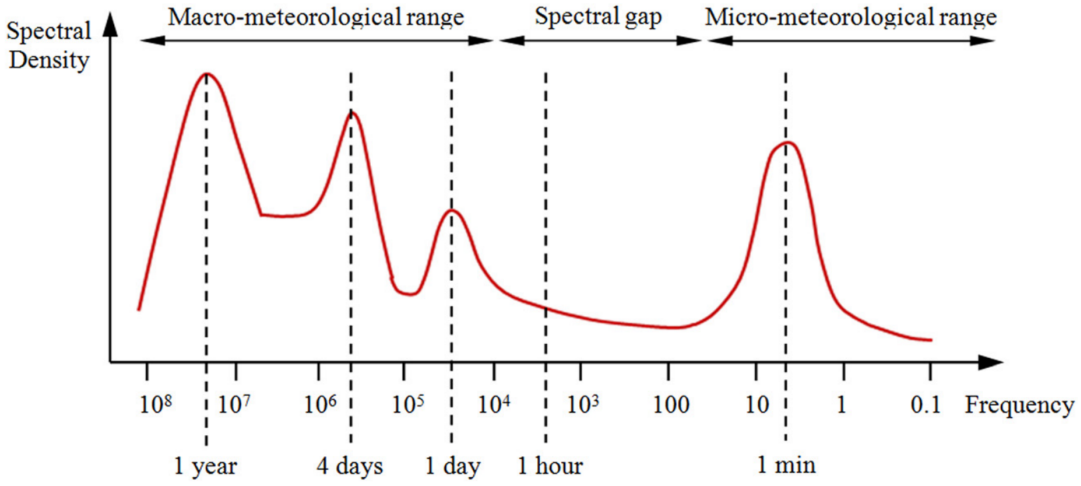

Figure 1.6: Wind Spectrum

The wind has four principal frequencies of variation. The quickest variation happens at intervals of 20-60 seconds. In the quicker intervals, the blade pitch control is too slow to dissipate all additional energy, and the transmission is suspect to damage. If the energy from short bursts of wind was stored temporarily instead of mitigated by blade pitch, and later re-added to the system, the system would become more reliable. This is accomplished with hybridization of the transmission.

1.7 Hybrid System

A hybrid system is any system that contains more than one form of power, typically including at least one form of energy storage. The goal of energy storage is to take

the additional power that would be intentionally dissipated in region 3, and store it temporarily. When the wind speed decreases back into region 2, the stored energy is released to increase the power captured. A successful Energy Storage System (ESS) will remove additional energy quickly from the transmission without using blade pitch control to limit power. This increases the total power produced. This is illustrated in Figure 1.7.

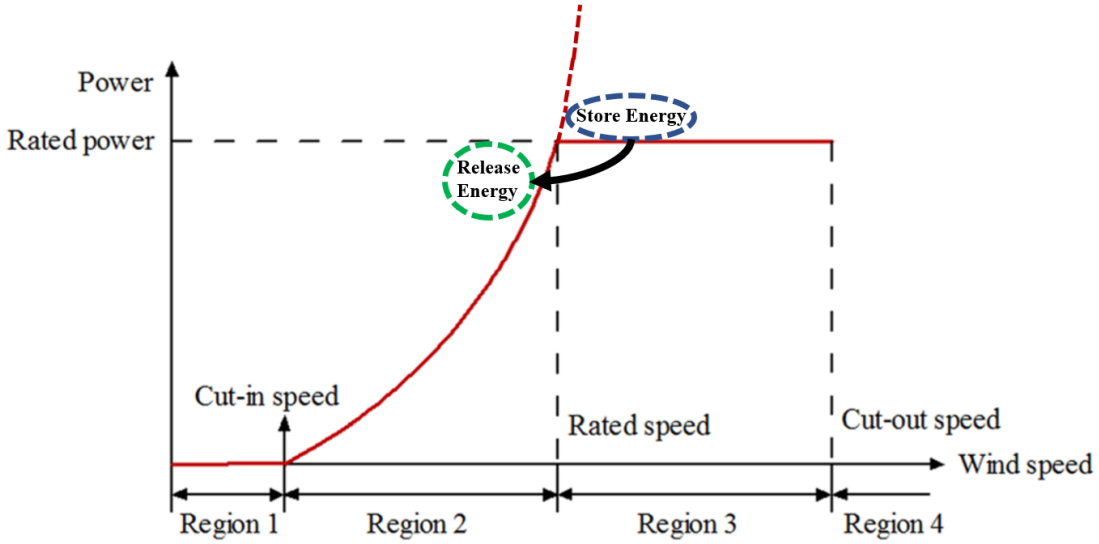

Figure 1.7: Hybrid System Storage Goal

Energy is stored for a short period of high wind speeds, and then released back into the transmission when the wind speeds are lower than rated. If sufficient at removing energy, the system can operate the turbine transmission at its constant rated power for extended periods of time. This increases the total amount of energy produced, increases transmission reliability, and offers a quick response time for brief gusts of wind. If sized

properly, an ESS can keep the transmission running smoothly near the constant power for extended periods of time when wind speeds are varying around the rated speed.

Wind turbines operate at high power and have a high inertia. During high wind speeds, power has to be removed quickly, and during low wind speeds, power has to be added quickly. Hydraulic accumulators are one of the most power-dense energy storage components. They can store energy quickly at high power and quickly add energy with high power, even with a high inertia system.

Hydraulic ESS's have been previously researched by many groups and found useful in high power applications. Successful applications typically have a dependable duty cycle and are high power, such as hydraulic hybrid vehicles, forklifts, and garbage trucks [18]. Hydraulic hybrid systems are also a blossoming prospect in the off-road and agriculture industry, where high power is a necessity [19].

Although they are high power, wind turbines have a less dependable duty cycle. This has led to alternate forms of ESS's being investigated for wind turbines. These include pumped hydro-storage, flywheel energy storage, and compressed air energy storage systems [20]. These systems have their benefits, but none can match the amount of power provided by the hydraulic system. Some projects also focus on long-term energy storage systems in order to store energy for hours or days to create a smoother long-term period of operation [21]. This research instead focuses on short periods of energy storage to create a smooth power output. A hydraulic ESS has been previously investigated for short-term energy storage [22]. The previous project placed an ESS on the high-speed

shaft of the transmission. The current research instead places the ESS on the low speed shaft of the transmission to increase system reliability.

The high power of the accumulator is essential for providing ancillary benefits of the hybrid system. When there is a fault in the power grid, energy from the accumulator can be rapidly released at high power to maintain proper grid operation for short faults. The high power in the accumulator can also be used to pitch turbine blades and yaw during severe weather.

1.8 Research Objective

The goal of this research project is to improve the quality of mid-size wind turbine transmissions. This is done by creating a high-power ESS that can add or remove power from the turbine transmission to create a smooth output power that hovers at the rated power for longer periods of time. The resulting system can increase the annual energy produced while maintaining and potentially improving the reliability of the turbine transmission. More continuous operation near the rated power during turbulent wind can lead to a higher quality of produced electricity [23] .

1.8.1 Key Contributions

- Design, modeling, and control of a novel hybrid hydraulic energy storage system for mid-size HST wind turbine transmissions.
- Large-scale hardware upgrade of a power regenerative test platform.
- Experimental characterization of system losses and accumulator behavior.
- Experimental validation of high-fidelity dynamic model of the hybrid system.
- Prediction of effectiveness of the hybrid system, including additional annual energy production.

1.9 Chapter Overview

This thesis is divided into four chapters. In chapter 2, the design and modeling, control, and preliminary simulation of the hybrid system are discussed. In chapter 3, the design of an upgrade to the power regenerative HST test platform at the University of Minnesota is discussed [24]. In chapter 4, the simulation is experimentally validated, and characterization experiments are used to improve fidelity. In chapter 5, the results and implications of the system are discussed and conclusions are drawn.

Chapter 2

Hybrid System Design, Modelling, Control, and Preliminary Simulation

2.1 Hybrid System Architecture

The designed hybrid system architecture is shown in Figure 2.1.

Outside of the red dashed box is a standard HST turbine as described in the introduction and shown in Figure 1.4. Inside the box is an ESS designed to hybridize the transmission. The ESS is an independent add-on to an HST and can be added to any type of wind turbine transmission. In this thesis, the ESS will be added to a HST due to previous evidence of the benefits of the HST, and the ability to perform experiments

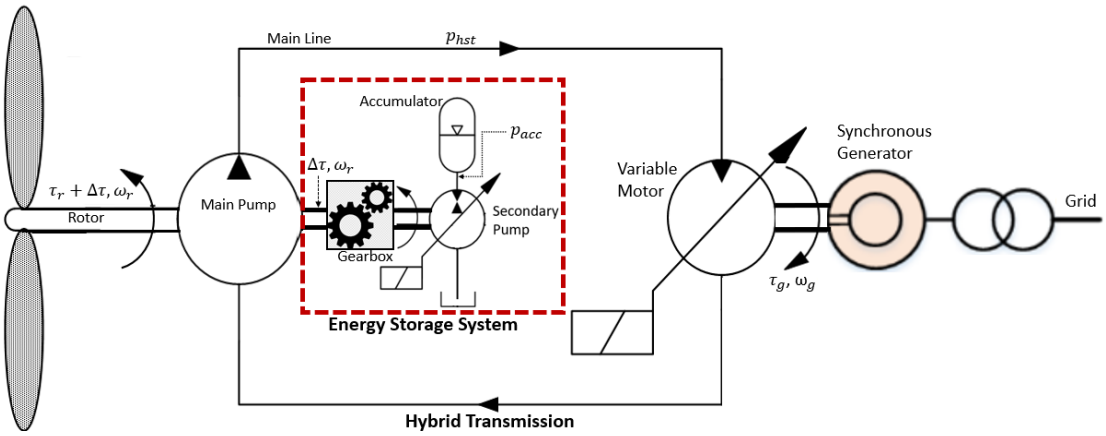

Figure 2.1: Hybrid System Architecture

on the power regenerative HST test platform at the University of Minnesota [24] [25] .

The ESS uses a gearbox, a variable-displacement pump called the secondary pump, and an accumulator to store energy. When active, the turbine rotor drives the secondary pump, which charges and discharges the accumulator. When wind speeds are above the rated speed, the rotor shaft takes on additional power from the wind $P_{rot} = P_r + \Delta P$. The rated power, P_r is transmitted to the grid through the HST, and the additional power, ΔP, is transmitted to the accumulator by the secondary pump. When wind speeds are below rated, ΔP is negative. The stored energy in the accumulator is used to supply power to the HST through the secondary pump and rotor. The secondary pump is designed to charge and discharge the accumulator with unidirectional rotation. The gearbox is used to make the secondary pump run at a more efficient speed, and allows the secondary pump to be smaller.

The ESS is placed on the low speed shaft to improve the system reliability. Wind

power increases with the cube of wind speed, so a small increase in wind speed above rated creates a large increase of power in the system. By placing the energy storage system on the low speed shaft, additional power is stored immediately at the input, and not transmitted throughout the transmission. This increases the overall system reliability. The resulting architecture is modeled.

2.2 Dynamic Modeling

To predict the performance of the hybrid transmission during different wind inputs, a high-fidelity dynamical model of the transmission was produced. The transmission is governed by rotor dynamics, HST pressure dynamics, and accumulator dynamics, as described in [26].

2.2.1 Rotor Dynamics

Dynamics for the rotor are found from the sum of applied torques on the shaft:

$$J_r\dot{\omega}_r = \tau_{rot}(\omega_r, u, \psi) - b_r\omega_r - D_{p1}p_{hst} - \gamma D_{p2}G_r p_{acc} \tag{2.1}$$

where J_r is the inertia, and b_r is the damping of the rotor shaft and main pump. τ_{rot} is the aerodynamic torque, which is a function of the rotor speed ω_r, the wind speed u, and the blade pitch angle ψ. D_{p1} is the displacement of the main pump, and D_{p2} is the displacement of the secondary pump. γ is the normalized swash plate angle of the secondary pump. p_{hst} is the pressure drop across the main pump, and p_{acc} is the

pressure in the accumulator.

2.2.2 Pressure Dynamics

Dynamics of the HST pressure are found from the sum of flows into the control volume of the high pressure line of the HST:

$$\dot{p}_{hst} = \frac{\beta_e}{V}[D_{p1}\omega_r - L_m p_{hst} - \alpha D_m \omega_g] \tag{2.2}$$

where V is the fluid line volume. L_m is the combined losses of the motor and the main pump, assuming no losses in the line. D_m is the displacement of the motor. α is the normalized swash plate angle of the motor. β_e is the effective bulk modulus of the fluid and line, linearized at operating line pressure p_{hst}.

2.2.3 Accumulator Dynamics

Dynamics of the accumulator are found from the sum of flows into the control volume of the accumulator:

$$K_{acc}\dot{p}_{acc} = \gamma D_{p2} G_r \omega_r - L_{p2} p_{acc} \tag{2.3}$$

where L_{p2} is the flow loss term of the secondary pump. K_{acc} is not a constant, but rather a non-linear, time-changing variable that represents the instantaneous relationship between the flow rate of fluid into the accumulator and the pressure of the accumulator. This value depends on the modeling method of the accumulator.

2.3 Accumulator Modeling

Accumulator modeling presents challenges depending on the rate at which the accumulator charges [27]. Every accumulator has a thermal time constant dependent on the size and material. When an accumulator charges significantly faster than its thermal time constant, the process is considered to be adiabatic. When an accumulator charges significantly slower than its thermal time constant, the process is considered isothermal. Both are lossless processes. When an accumulator charges in a time close to the thermal time constant, it is important to include a model that includes losses. In many hydraulic systems, accumulators charge and discharge in times typically less than 10 seconds, and an adiabatic model is used. However, in this system the duty cycle is unpredictable. All three models are investigated.

2.3.1 Adiabatic and Isothermal

Adiabatic and isothermal models are lossless models. An adiabatic model assumes that there is no heat loss during the compression and expansion of a gas, or the charging and discharging of a gas bladder accumulator. This assumption is valid when an accumulator charges significantly faster than its thermal time constant. From the first law of thermodynamics, the adiabatic gas equation is derived as:

$$pV^n = p_0V_0^n = C_{adi} \tag{2.4}$$

Where p and V are the pressure and volume of the accumulator gas at any given

time, p_0 and V_0 are the precharge gas pressure and volume, and n is the polytropic index, typically 1.4 for N2 gas, used in the adiabatic model, and C_{adi} is the adiabatic process constant. By taking the first-order derivative of the adiabatic equation, the resulting relation between accumulator pressure and the flow rate into the accumulator is produced:

$$\frac{dp_{acc}}{dt} = \frac{np_{acc}^{1+\frac{1}{n}}}{C^{\frac{1}{n}}\frac{dV_acc}{dt}} \tag{2.5}$$

Where p_{acc} and V_{acc} are the accumulator fluid pressure and volume. Note that this equation relates the flow into the accumulator to the rate change in pressure of the accumulator, similar to equation 2.3. The value of the accumulator constant K_{acc} for an adiabatic process is found as:

$$K_{acc} = \frac{C_{adi}^{\frac{1}{n}}}{np_{acc}^{1+\frac{1}{n}}} \tag{2.6}$$

An isothermal process is one in which the temperature stays constant during the charging and discharging process. This assumption is valid when an accumulator charges significantly slower than its thermal time constant. It can be shown by the first law of thermodynamics that this is equivalent to the adiabatic gas equation with a value of $n = 1$. By using the same method of taking the first-order derivative of the gas equation, the value of K_{acc} can be found to be:

$$K_{acc} = \frac{C_{iso}}{p_{acc}^2} \tag{2.7}$$

Noting that the value of C_{iso} is $p_0 V_0 = C$

2.3.2 Heat Transfer Method

The heat transfer model lies between the isothermal and adiabatic models. The model does not assume a lossless process. Instead, the relationship between the pressure of the accumulator and the flow rate of fluid is determined by a second-order transfer function. Otis developed this model by performing an energy balance on the accumulator gas [27]. Through simplification and the assumption of small perturbations in pressure as detailed by Otis, the resulting transfer function is [27]:

$$p_a cc = \frac{p_0}{V_0} \frac{1 + n\tau s}{V_0 s(1 + \tau s)} \frac{dV_{acc}}{dt} \tag{2.8}$$

Where n is the ratio of specific heats of the gas, also used in the polytropic equation, s is the frequency domain operator, and τ is the thermal time constant, specific to each accumulator. The estimate provided by Otis [28] is used:

$$\tau = \frac{m_g c_v}{h A_w} \tag{2.9}$$

Where m_g is the mass of the gas in the accumulator, c_v is the constant volume specific heat, A_w is the area of the accumulator walls, and h is the heat transfer coefficient. Using the estimate value of τ assumes the accumulator is charged with an ideal gas. Alternatively, the Benedict–Webb–Rubin (BWR) real gas equation can be used [29]. To find an appropriate value of the heat transfer coefficient, h , a basic heat transfer model

of forced convection on the interior of a cylinder was used [30]. To more accurately get this value, experimentation of the accumulator is needed.

This approach is only valid for small perturbations in pressure and volume near the precharge values. Since the accumulator for the hybrid system will have larger perturbations, the transfer function is actively linearized near the volume and pressure at the previous step in time, giving the final equation, first used in [31]:

$$\Delta p_{acc} = \frac{p_{acc,t-\Delta t}}{V_{acc,t-\Delta t}} \frac{1+\gamma\tau s}{s(1+\tau s)} \frac{dV_{acc}}{dt} \tag{2.10}$$

Where Δt is the sampling frequency of the simulation. The change in pressure calculated is then added to the pressure at step $t - \Delta t$ to get the new pressure.

With an understanding of the system dynamics, control of the system is discussed.

2.4 Control

The goal of the energy storage system is to maintain the HST near a constant rated operation when wind speeds are varying near the rated speed. This works by removing and supplying power to the HST. It is necessary to ensure that control of the ESS does not interfere with the control of the HST or HST test platform. The hybrid system from equations 2.1, 2.2, and 2.3 is a non-linear MIMO system with three inputs and three outputs. When dynamics of the test platform are included, it becomes more complicated. To ensure the ESS is independent, measurements and references for the controller must not threaten the stability of the HST or test platform.

2.4.1 HST Turbine Standard Control

In conventional HST turbines, the control scheme is straight-forward. In regions 1 and 4, the system is disabled. In regions 2 and 3, the power captured is maximized. In region 3, blade pitch control is used to limit the power, but the same control strategy for the HST motor can be used. The control strategy is the Kω^2 law, which is a commonly used turbine control strategy [32]. The rotor speed is measured and an optimal reference torque is generated based off of the turbines ideal tip speed ratio, λ^*.

$$\tau_{ideal} = K\omega_r^2; K = \frac{\pi\rho R^5 Cp_{max}}{2\lambda^*} \tag{2.11}$$

Where ρ is the density of air, R is the blade radius, and Cp_{max} is the maximum power coefficient for the specific turbine.

The HST motor swash plate angle is changed to adjust the system pressure to ensure the optimal rotor torque is achieved, maximizing power capture. This strategy is simple and efficient, and only requires measurement of the rotor speed and knowledge about the turbine's physical characteristics.

2.4.2 Hybrid System Control

The inputs for the hybrid system are the variable motor displacement, the secondary pump displacement, and the wind torque. The wind torque depends on the wind speed, the rotor speed, and the blade pitch angle of the turbine. Since the wind speed is not controllable, and the rotor speed is a state, the third control input is the blade pitch angle. The outputs of interest are the three states, ω_r, p_{hst}, and p_{acc}.

The hybrid system's desired operation is described in four distinct modes. These modes depend on the wind speed and the amount of stored energy in the accumulator. When the wind speed is lower than rated speed and there is no energy stored in the accumulator, the system is in mode I. The wind speed is in region 2, and standard power maximization control is implemented with a constant blade pitch and an inactive ESS. When the wind speed is lower than the rated speed and there is energy stored in the accumulator, the system is in mode II. The wind speed is in region 2, but power stored in the accumulator can be used to keep the turbine operating near its rated power for an extended period of time. The ESS becomes active and replenishes the HST with stored power while blade pitch is kept constant and the HST uses standard power-maximization control. When the wind speed is above the rated speed and the accumulator is not full, the system is in mode III. The wind speed is in region 3, but the accumulator can be used to store power to keep the turbine operating near its rated power. The ESS becomes active and removes energy from the HST by storing power while blade pitch is kept constant and the HST uses standard power-maximization control. When the wind speed is above the rated speed and the accumulator is full, the system is in mode IV. The wind speed is in region 3, but the accumulator is fully charged. Excess energy is dissipated with the blade pitch control strategy, while the ESS control becomes inactive and the HST uses standard power-maximization control.

The power level of the HST is based on HST control, which is always using $K\omega^2$ power-maximization control. This control measures the rotor speed as a reference. To

change the power of the HST without changing the HST controller, the rotor speed can be changed. The ESS controls the rotor speed to a desired value. The HST motor then delivers the maximum power at that rotor speed. The rotor speed is set to the rated speed, and the rated power is produced by HST motor control when needed.

By using the ESS control to adjust the reference for the HST control, the controllers will not interfere. The system has four distinct operating regions and three independent control inputs. To determine which of the four operating regions the hybrid system is in, the system must measure the wind speed and accumulator State Of Charge (SOC). The system must also measure the rotor speed. Measuring wind speed and accumulator volume are not easy nor reliable measurements. More reliable with a HST is measuring the HST and accumulator pressure. The HST pressure increases with wind speed, and the accumulator pressure correlates to the SOC via adiabatic or isothermal models. These measurements are cheaper, more accurate, and can be quickly measured. A summary of the control strategy for the hybrid system is shown in table 2.1.

Table 2.1: Rule Based Control

Mode	Line Pressure	Accumulator Charge	γ Control Strategy	Blade Pitch Control
I	$p_{hst} < p_{rated}$	SOC $= 0$	Center Swash Plate ($\gamma = 0$)	Maintain constant pitch
II	$p_{hst} < p_{rated}$	$0 <$ SOC ≤ 1	Discharge Accumulator ($\omega_{ref} = \omega_{rated}$)	Maintain constant pitch
III	$p_{hst} \geq p_{rated}$	$0 \leq$ SOC < 1	Charge Accumulator ($\omega_{ref} = \omega_{rated}$)	Maintain constant pitch
IV	$p_{hst} \geq p_{rated}$	SOC $= 1$	Center Swash Plate ($\gamma = 0$)	Pitch to remove energy

The rules are defined by single point values, but there are sometimes errors in measurement. This can lead to the system rapidly switching between rules. To combat this, a fifth mode was created.

2.4.3 Controller Mode V

When the system control was initially tested, it was found that the swash plate angle would encounter a rapid switching phenomenon. This happens because of noise caused by vibrations of the real system and instrumentation noise. When the wind speed is right near rated, this noise can cause the system to rapidly switch between regions of control.

A fifth mode was added to the rule based control. This mode is referred to as mode V. In mode V, the wind speed is close to rated speed. The swash plate angle is set to zero, regardless of the accumulator pressure. In this small zone, the large inertia of the

rotor keeps the HST operating near rated with minimal shock loading while the ESS is inactive. When additional power is introduced, the system leaves the mode V zone and returns to normal operation. This fixes the fast switching between operation modes. The additional rule is summarized in Table 2.2.

Table 2.2: Mode V

Mode	Line Pressure	γ Control Strategy	Blade Pitch Control
V	$p_{rated} + \Delta p \geq p_{hst} \geq p_{rated} - \Delta p$	Center Swash Plate ($\gamma = 0$)	P Maintain constant pitch

Where Δp is half of the Mode V zone width, found experimentally to work well at 4 bar. HST control for the HST has been established in previous work to be stable with a PI control [33]. Blade pitch control is artificially added to the simulation and the experiments via first-order transfer function, which is stable. The secondary swash plate controller measures the error between rotor speed and the rated rotor speed and uses a negative proportional gain. This is found to be stable for a limited range of proportional gains. The stability of the ESS controller is verified in Appendix A. A preliminary simulation of the system is run to verify the controller works properly in a nonlinear situation.

Table 2.3: Turbine and Simulation Parameters

Parameter	Value	Unit
Rated Power	60	kW
Rated Wind Speed	10	$\frac{m}{s}$
Blade Radius	10.6	m
Optimum Power Coefficient	0.41	—
Optimum Tip Speed Ratio	6.5	—
D_{P1}	2512	$\frac{cc}{rev}$
D_m	135	$\frac{cc}{rev}$
D_{P2}	55	$\frac{cc}{rev}$
G_r	30	-
V_{acc}	50	$liters$
$p_{acc,max}$	350	bar
$V_{acc,max}$	50	$liters$
$p_{acc,0}$	125	bar

2.5 Preliminary Simulation

The system modeling and controller design were implemented in a preliminary simulation to better understand the system. The dynamic model described in equation 2.1, 2.2, and 2.3 with the aforementioned controller are simulated with Simulink for a 60 kW Polaris turbine. Turbine characteristics and simulation parameters are shown in Table 2.3.

The hybrid simulation is compared to a conventional HST transmission turbine with instantaneous blade pitch. A series of wind input steps is simulated and shown in Figure 2.2.

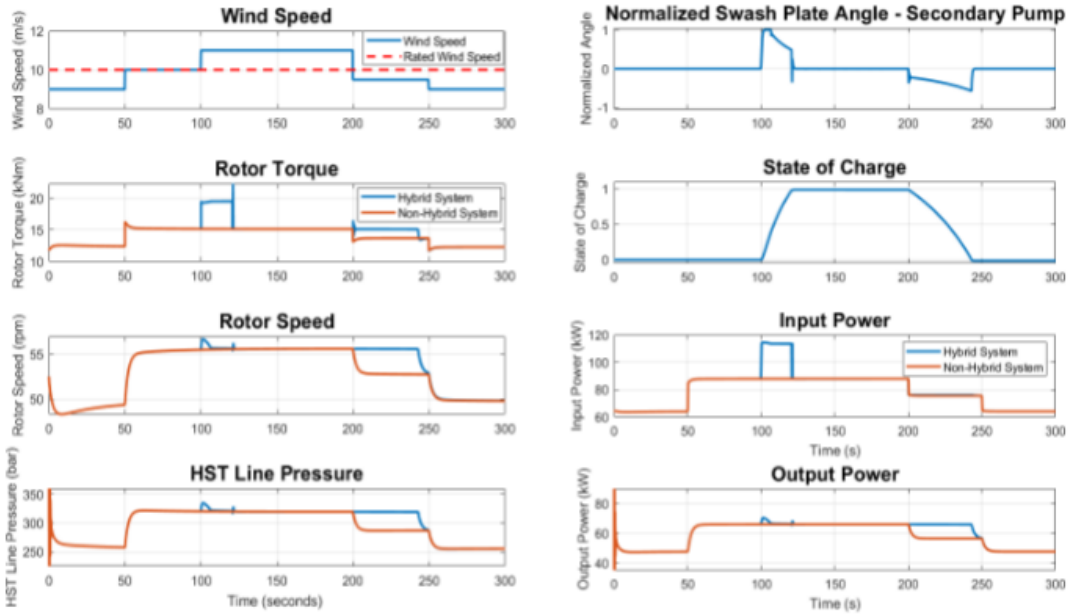

Figure 2.2: Preliminary Simulation Results

From 0 to 100 seconds, the wind speed is in region 2, and the system is in mode I. The energy storage system is inactive and the hybrid and non-hybrid systems have identical rotor torque, speed, and HST pressure. The input and output power match. From 100-120 seconds, the wind speed is in region 3, and the system is in mode III. The wind is higher than the rated wind speed, and the accumulator begins to charge, removing energy from the HST. The secondary swash plate controls the rotor speed to the rated rotor speed, and HST power maximization control maintains the system at the rated pressure. The non-hybrid system pitches its blades to maintain the input power at rated. Meanwhile, the hybrid system does not pitch its blades. Instead, the input power is allowed to increase. Due to the ESS, the output power remains at the rated power. From 120-200 seconds, the wind speeds are in region 3, and the system is in mode IV. The wind is higher than the rated wind speed and the accumulator is full. Both hybrid and non-hybrid systems use blade pitch control to mitigate damage to the transmission. Once again, the hybrid and non-hybrid systems have identical rotor torque, speed and HST pressure, and the input and output power match. From 200-250 seconds, the wind speeds are in region 2 and the system is in mode II. The wind speeds are below rated and the accumulator is not empty. The ESS adds power to the HST to maintain operation at the rated power for an additional 40 seconds.

This illustrative example shows the hybrid system in action. By allowing additional power to be captured and stored in the accumulator, more energy can be produced by the hybrid system over a given period than the non-hybrid system. With a greater

understanding of how the hybrid transmission will work in simulation, experiments were performed to validate and expand upon the simulation results. To perform the experiment, an upgraded test platform was built. In the next section, the design and instrumentation of the upgraded hybrid HST test platform is detailed.

Chapter 3

Hardware Modification

To perform the experiments, the hybrid system was built. The ESS can be added to any wind turbine transmission to make the system hybrid. The power regenerative HST test platform at the University of Minnesota is an elaborate HST testing platform used for HST wind turbine testing [25]. The HST platform was modified to include the ESS for hybrid testing.

3.1 HST Test Stand

The HST power regenerative test platform at the University of Minnesota is shown in Figure 3.1. This platform consists of a speed-up and speed-down HST that runs in a loop with a 55 kW electric motor to start up and replenish losses in the system. This allows the test platform to run as a 100 kW transmission.

This bed has been previously developed to perform a multitude of tests [25]. The

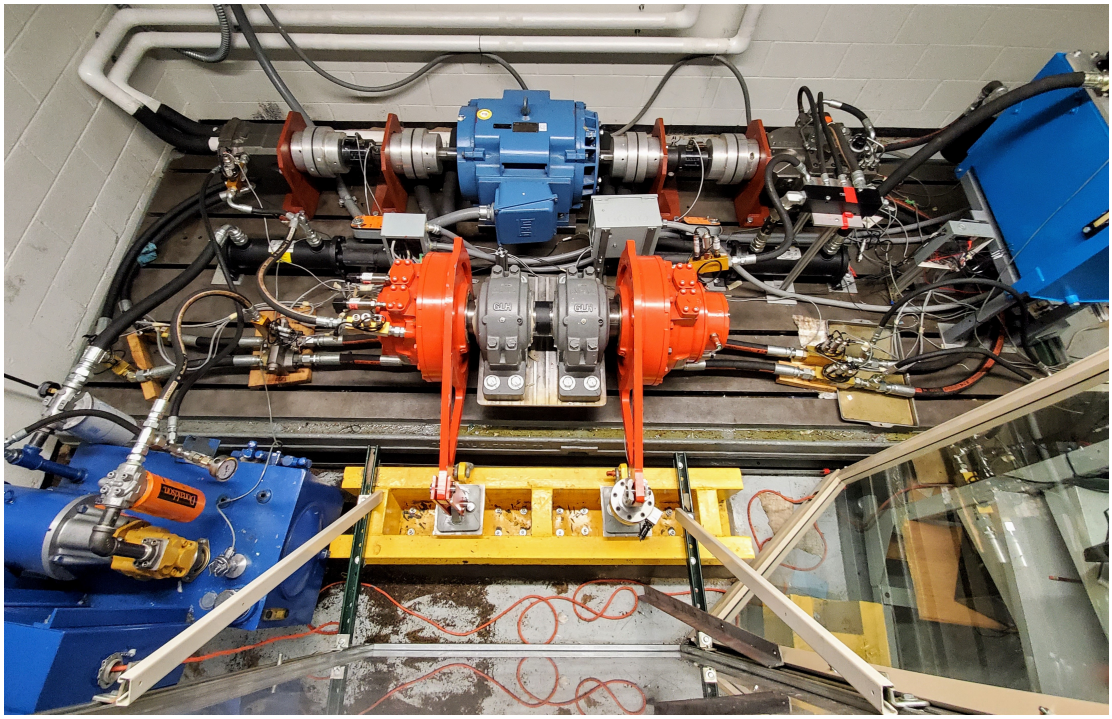

Figure 3.1: Power Regenerative HST Test Platform

speed-down HST on the right hand side is integrated with hardware-in-the-loop simulation to create realistic wind loading conditions on the rotor shaft. The speed-up HST on the left hand side is used to collect data. In this thesis, the speed-down HST is referred to as a HydroStatic Drive (HSD) because it acts as the power source for hybrid system testing. The speed-up HST is referred to as the HST, as it is the HST that is used in the wind turbine transmission. With the advanced control strategy of the test bed, the system can be used in multiple ways. The HSD pressure, high speed shaft speed, and rotor speed are controllable. Alternatively, a wind speed input can be provided. The three control inputs are the VFD power, the HST motor swash plate angle, and the

HSD pump swash plate angle. This platform is upgraded with the addition of the ESS to create the hybrid system.

3.2 Hybrid Test Platform

Figure 3.2 shows the upgraded test platform, labeled with the major components of the new ESS.

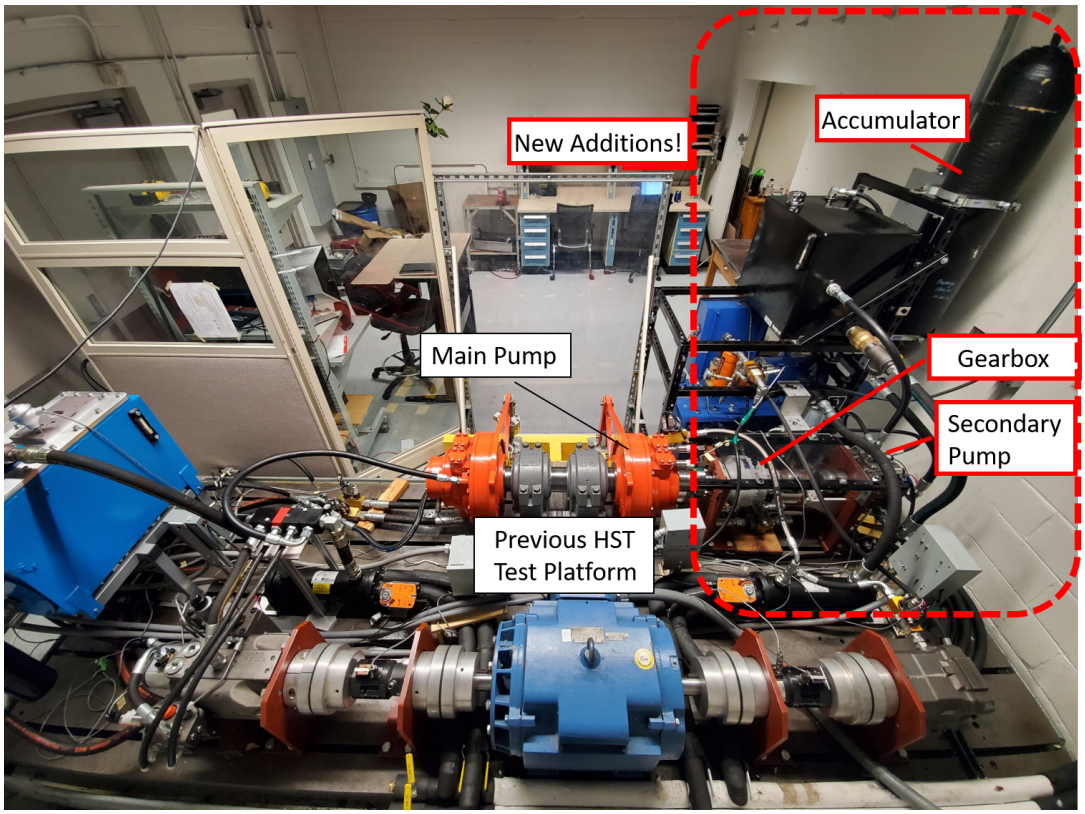

Figure 3.2: Upgraded Power Regenerative HST Test Platform

The upgraded system adds an independent hydraulic ESS. This allows the platform to perform hybrid transmission testing, but also perform accumulator and secondary

pump testing, as well as oil testing. The ESS cannot be easily disconnected from the test platform, but the secondary pump displacement can be controlled to minimize its presence. The platform can still operate without the ESS.

The main components of the ESS are the secondary pump, the gearbox, and the accumulator. The ESS adds 5 additional sensors, including the torque and speed of the high-speed storage shaft, as well as the pressure and temperature of the accumulator, and the flow rate in and out of the accumulator. Each major component of the ESS has major implications for the design of the system.

3.2.1 Accumulator

Accumulators vary in type, volume, and maximum pressure. For the bladder accumulator, the effect of changing the accumulator volume and maximum pressure was simulated. This was a preliminary simulation designed to help select the accumulator. The amount of additional energy produced compared to a conventional system for a standard turbulent wind model was measured, and results are shown in Figure 3.3.

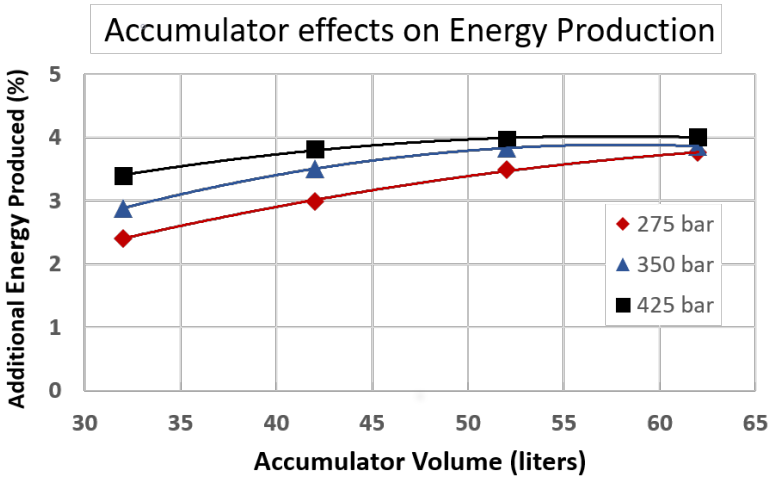

Figure 3.3: Accumulator Sizing

The preliminary results showed that the amount of additional energy that can be stored increases with accumulator size and maximum pressure. However, the benefits of an increased size and pressure are limited. This means there is a theoretical optimal size once the cost is considered. Further cost analysis versus benefit analysis was not performed. A 350 bar, 52 L bladder accumulator was selected because it is within reasonable range of the theoretical optimum accumulator size and pressure, and was already donated to the university. The unit is a Hydac SB345-50F1/693U-345D carbon fiber accumulator.

Bladder accumulators also have an adjustable precharge pressure. For energy storage, the theoretical optimal precharge pressure is 1/2.67x the maximum pressure [34]. The precharge pressure value greatly effects the adiabatic or isothermal constants, and is important for the heat transfer model. This variable is explored in the results section.

3.2.2 Secondary Pump

The secondary pump must operate in a nonstandard way. It must act as a pump while charging the accumulator, and a motor while discharging, yet in a wind turbine, the rotor will exclusively rotate in one direction. To do this with one port connected to tank and the other connected to the accumulator, the internal swash plate needs to turn to positive and negative angles. When the ESS is not in use, the turning losses need to be minimized, and the swash plate angle is set to zero. Figure 3.4 shows the three modes of operation for the secondary pump.

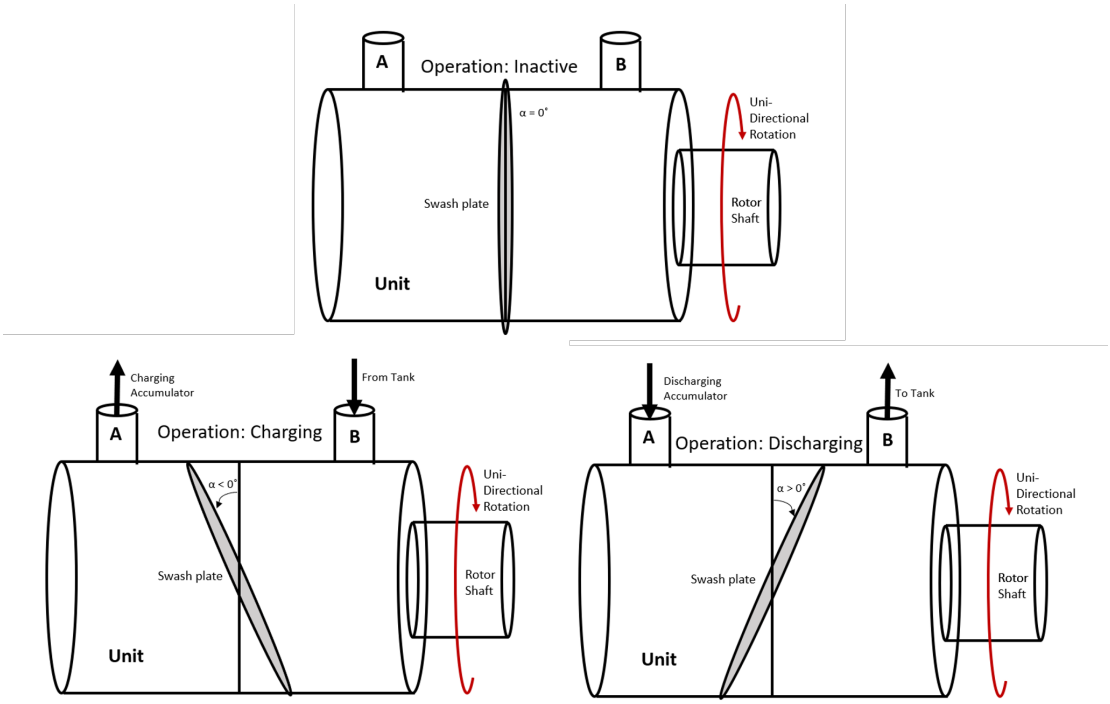

Figure 3.4: Secondary Pump Modes of Operation

The only market-available units that have this swash plate operation are high pressure variable piston pumps. The Linde HPV-02 HPV055LIE1PC10D5CC3509R19XXAX2X pump was selected. This is a closed-loop pump that is designed for high pressure and four-quadrant operation, which provides the desired operation for the ESS.

3.2.3 Gearbox

The secondary pump was selected for its modes of operation, however, there is a market gap in high pressure, four-quadrant pumps that can run at a low speed. To have the secondary pump run at the speeds it is designed for, a 30:1 two-stage planetary gearbox is selected. The gearbox is a Bonfiglioli 305 L2 30.8 gearbox. This unit is a compact gearbox designed for a high speed input and a high torque output, typically used in wheel loader applications. This unit is the part of the ESS that is most prone to damage and has a lower maximum power than the accumulator or secondary pump. To ensure the gearbox doesn't face extreme loading conditions a special additional control strategy was added. The control is described in Appendix B.

3.2.4 Clutch

One of the concerns with the hybrid system is that there will be parasitic losses when the ESS is inactive due to the constant turning of the gearbox and secondary pump. One way to compensate for this is by adding a clutch that can decouple the shaft when the system is inactive. The losses are difficult to model without experimentation. Due

to space concerns, the clutch was not added, but is potentially an important part of the system and will be explored in the results section.

3.3 ESS Design

The ESS must include the above components, but also faces more complications in the design. The shaft for the ESS required careful thought in its construction to avoid shaft imbalance, misalignment, or overconstraint. Details of the final design are shown in Appendix C. In the ESS shaft design, special mounting plates, a special adapter, and a torque sensor mount were designed, as shown in Appendix D.

The ESS runs on an independent hydraulic circuit. The details of this hydraulic circuit are described in Appendix F. When developing the test platform, there were two potential major issues that needed to be addressed. This includes a cavitation concern in the secondary pump, and an inability to control the secondary pump swash plate because of a lack of pilot pressure. The cavitation concern is addressed with a large inlet line, and an elevated tank, and careful pressure monitoring. The pilot pressure concern is addressed by modification of an internal valve in the secondary pump. These two problems are detailed in Appendix G. The secondary pump also requires a driver to operate. The details of this driver are shown in Appendix H.

3.4 Instrumentation

The energy storage system includes 5 dedicated sensors. These measure the torque and speed of the high speed storage shaft, as well as the pressure and temperature of the accumulator, and the flow rate in and out of the accumulator. The list of sensors, outputs, and their uncertainties are summarized in Table 3.1. More details on sensor and uncertainty analysis are found in Appendix I.

Table 3.1: Sensors

Sensor	Unit	Output Signal	Uncertainty
Acc Pressure	Bar	4-20 mA	1.43%
Acc Flow	gpm	0-5 VDC	1.29%
Acc Temp	C	4-20 mA	1.43%
ESS Torque	Nm	4-20 mA	0.54%
ESS Speed	rpm	TTL	0.33%

Chapter 4

Experimental Results

Once the hybrid test platform was functional, a number of experiments were performed to test the effectiveness of the hybrid system. Experiments were conducted to measure the losses of the ESS, characterize the accumulator, and evaluate performance in step and turbulent wind conditions. This data is then used to predict the total amount of additional annual energy the turbine can produce. To ensure high quality data, the test bed was run for 10 hours to ensure air had been removed from the hydraulic lines, and that the new components were broken into steady operation. There is no temperature control in the ESS, so a period of 4 hours was given between any experiments to allow fluid to return to room temperature. The accumulator was charged and discharged several times before each data recording to ensure no air was entrapped.

4.1 ESS Loss Characterization

When the ESS is inactive, the system is still connected to the rotor shaft. The charge pump continues to run and the gearbox continues to turn. The secondary pump swash plate angle is set to zero, and the load caused by the energy storage system is minimized, but not negated. The system has additional damping and inertia. To determine the amount of losses this can have on the system, data for steady state operation of the test bed was recorded before and after the modification of the test platform at several wind speeds. In the hybrid experiment, the secondary swash plate angle was set to zero. The test platform will always provide the HST with the required power, so losses are characterized by the additional power needed in the HSD to provide the reference power. The HSD power is shown for the HST and the Hybrid System at several steady state wind speeds and is shown in Figure 4.1.

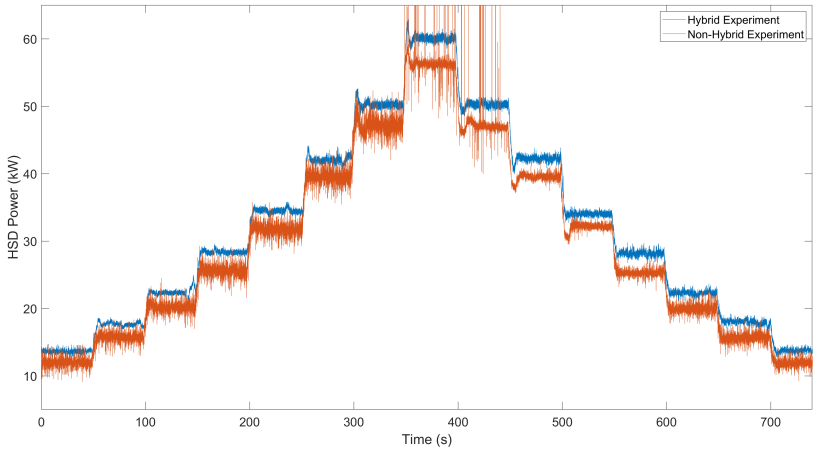

Figure 4.1: HSD Power

The hybrid system shows an increase in required HSD power to maintain a desired wind speed. This is because of the additional ESS inertia and damping. These values can be approximated by adding additional inertia and damping to the rotor inertia and damping, J_r, b_r from equation 2.1. Since the inertia of the turbine rotor is already large, the addition of the ESS will not have a significant impact on the inertia, and is neglected. The damping will have a more significant impact.

At each wind step the steady state speed and torque measured by the HST is subtracted from the speed and torque provided by the HSD. Since the rotor is at a constant speed, the result is the amount of torque lost due to damping. This loss consists of a static damping and a dynamic damping.

The torque lost to damping is plotted at various steady state wind speeds for the non-hybrid system in Figure 4.3.

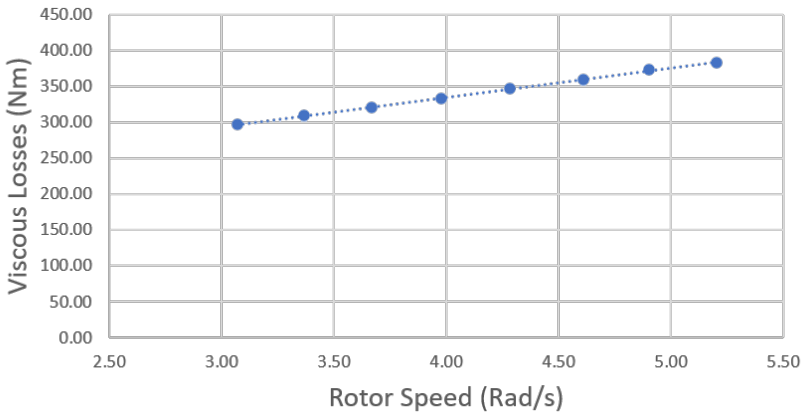

Figure 4.2: HST System

The same wind sample was used as an input to the hybrid system with the swash

plate angle set to zero.The resulting losses as a function of rotor speed are plotted in Figure 4.3.

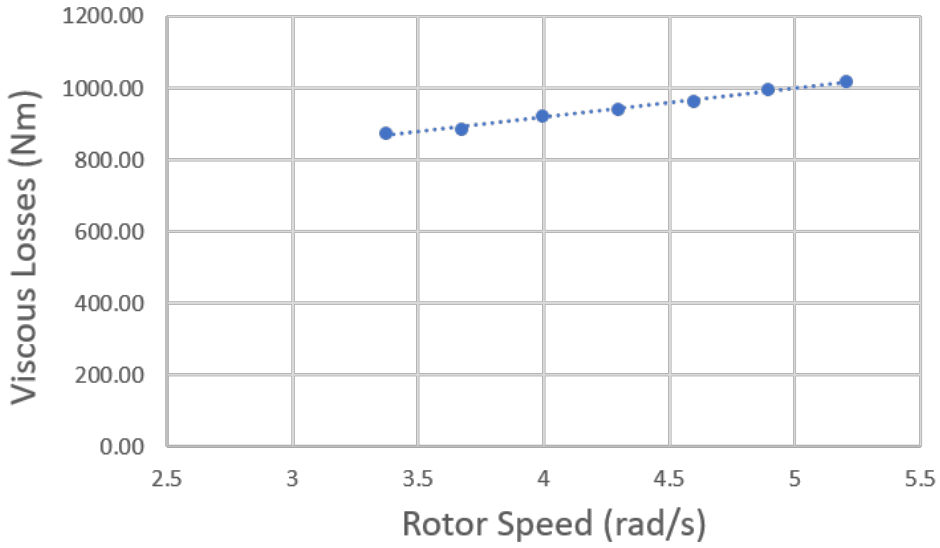

Figure 4.3: Hybrid System with Zero Displacement

The resulting slope, or rotor damping, is 82.2 Nm, just over double the damping of the non-hybrid system. The magnitude of the damping is also biased by an intercept of 400 Nm. This is the additional static torque. Because the secondary pump needs a charge pump, and the charge pump will create a constant flow run over a relief valve set to 20 bar, there is a parasitic torque equal to:

$$\tau_{charge} = D_{p,Charge} p_{Charge} = 140 Nm \tag{4.1}$$

The rest of the static torque addition could be attributed to bearing re-tolerancing. Regardless, the new value of b_r was updated in the simulation, and the additional constant torque term was added to the simulation to improve simulation fidelity. These

losses are undesirable. The addition of a clutch would remove the shaft during periods of inactive use, removing the constant torque term and minimizing the additional damping term.

4.2 Accumulator Experiments

The accumulator is a pivotal part of the ESS, and has significant effects on how much energy can be removed or added to the system. In order to understand the benefits of the ESS, the accumulator is characterized for simulation. A benefit of the modified test platform is that it allows for direct accumulator testing. By setting a constant rotor speed, the swash plate angle γ can be controlled to create a desired flow rate in or out of the accumulator.

4.2.1 Characterizing Accumulator Model Constants

The accumulator is characterized by the precharge pressure and gas volume. These factors determine the adiabatic and isothermal constants, C_{adi}, C_{iso}, and define parts of the heat transfer model. The accumulator is a 50 liter accumulator, precharged to 45 bar. However this value can change with age as the rubber bladder can harden and shrink [35]. The gas volume cannot be measured directly. Instead, the accumulator pressure was set to 75, 100, and 125 bar. The difference in tank volume was measured between these steps. The adiabatic and isothermal constants were varied above and below their estimated values. The resulting plots of gas volume verses accumulator

pressure are shown for the adiabatic case in Figure 4.4.

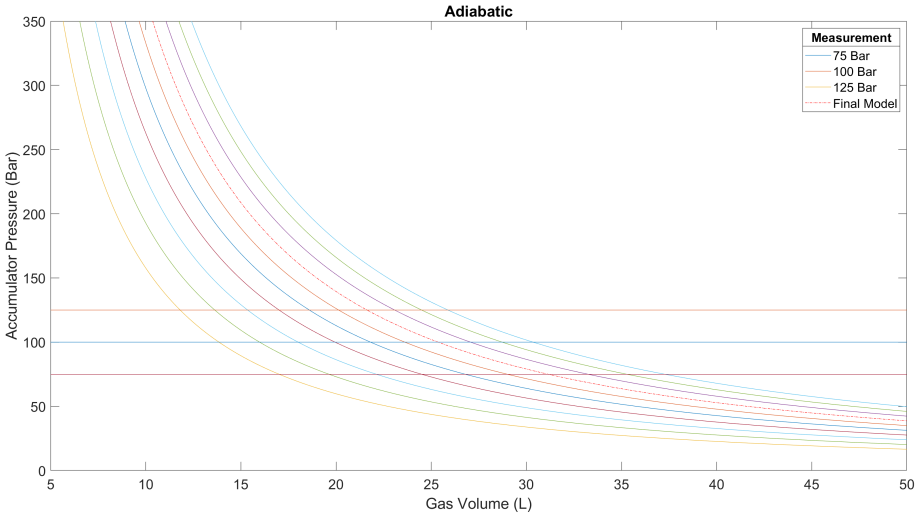

Figure 4.4: Characterization of Accumulator Model Constants

The arced lines are the lines of a constant adiabatic constant, C_{adi}. The horizontal lines are the lines at the three measured pressures. The distance on the X axis between two points in which an arced line and a horizontal line cross is the difference in volume. The two differences in volume are known between 75 and 100 bar, and 100 and 125 bar. By comparing those differences to the arced lines, the most accurate accumulator constant is determined. With this method it was found that a precharge pressure of 45 bar correlates to a maximum gas volume of 49 liters. This is used for the isothermal and heat transfer models. The resulting isothermal and adiabatic constants are:

$$C_{adi} = P_1 V_1^n = P_2 V_2^n = P_3 V_3^n \approx 60000 \tag{4.2}$$

$$C_{iso} = P_1 V_1 = P_2 V_2 = P_3 V_3 \approx 366000 \tag{4.3}$$

4.2.2 Characterization of Accumulator

To analyze the accumulator, the secondary pump swash plate angle was controlled to provide a constant flow rate. The rotor speed was set to 30 rpm, and the swash plate angle was adjusted to provide a flow rate of 4.0 Gpm in and out of the accumulator. The same flow rates were given as inputs to the simulation of the three accumulator models. The isothermal and adiabatic constants from equations 4.2 and 4.3 were used for their respective models. The heat transfer model uses initial conditions approximately equal to the adiabatic and isothermal models. Experimental results are shown in Figure 4.5 and overlaid with simulation results.

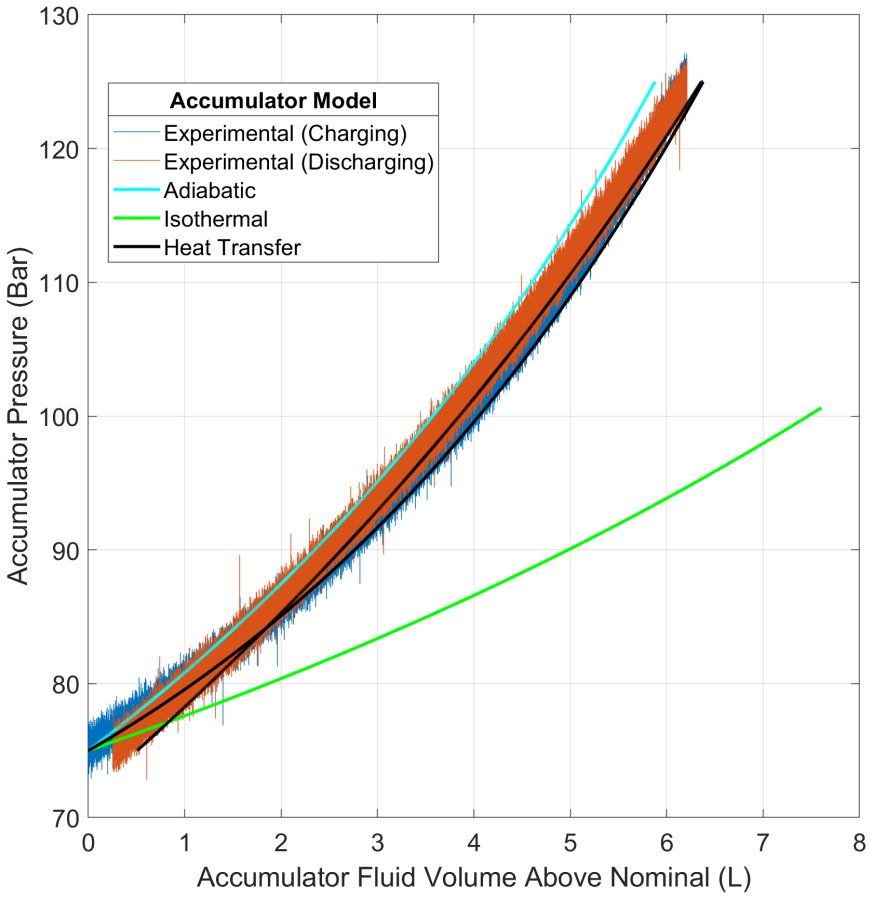

Figure 4.5: Characterization of Accumulator

The accumulator started at 75 bar and was charged to 125 bar, then discharged to 75 bar. The accumulator pressure is plotted against the fluid volume in the accumulator above the nominal fluid volume at 75 bar. The fluid volume was calculated by measuring time multiplied by the measured flow rate. In the adiabatic and isothermal simulations, the accumulator charges and discharges along the same line. This is because they are lossless models, and energy is conserved. In the heat transfer model simulation and the

experimental results, the accumulator charges and discharges on different lines. This indicates that some losses were incurred due to friction and heat transfer.

The real accumulator is not accurately represented by the isothermal model. Experimental results indicate the accumulator is close to both adiabatic and heat transfer models. However, experimental results show characteristics of the heat transfer simulation more so than the adiabatic simulation. Both real accumulator and heat transfer model build up pressure at a slower rate than they remove pressure. Since a near constant flow rate was provided, the fluid volume once the accumulator has returned to 75 bar will be higher. If allowed to fully discharge to nominal volume, the accumulator would read a lower pressure. The difference in pressure is the result of losses. The heat transfer model most accurately represents the experimental results.

The heat transfer model is dependent on the thermal time constant from equation 2.10. Based on the accumulator size, this time constant should be around 60 seconds. This is dependent on the heat transfer coefficient, h, which is not easy to predict. The value of h was varied to more accurately represent the actual thermal time constant. The adjusted thermal time constant, which is used in Figure 4.5, is found to be around 85 seconds. This heat transfer model is only an approximation due to the estimation of the thermal time constant. The accumulator was not instrumented with gas temperature measurement, which would allow for a more accurate way to verify the thermal time constant.

The real accumulator responds closer to different models depending on the rate the

accumulator charges as compared to its thermal time constant. If the accumulator charges significantly faster than its thermal time constant, it will act closer to the adiabatic model, and if the accumulator charges significantly slower than its thermal time constant, it will act closer to the isothermal model. The heat transfer model incorporates the thermal time constant and acts more adiabatic or isothermal depending on the rate of charging. At the flow rate in Figure 4.5, the accumulator charges in 25 seconds, significantly faster than its thermal time constant of 85 seconds, and the accumulator and heat transfer model act close to the adiabatic model. To test the robustness of the heat transfer model, more experiments were performed and compared to the simulation.

For this experiment, the rotor speed was set to 30 rpm, and the normalized swash plate angle γ was varied from $-0.35 < \gamma 0.35$. Figure 4.6 shows these charging and discharging cycles. A negative swash plate angle γ correlates to the charging of the accumulator, and a negative flow rate correlates to flow going into the accumulator. The accumulator pressure builds in a similar way to Figure 4.5 for each different constant flow rate.

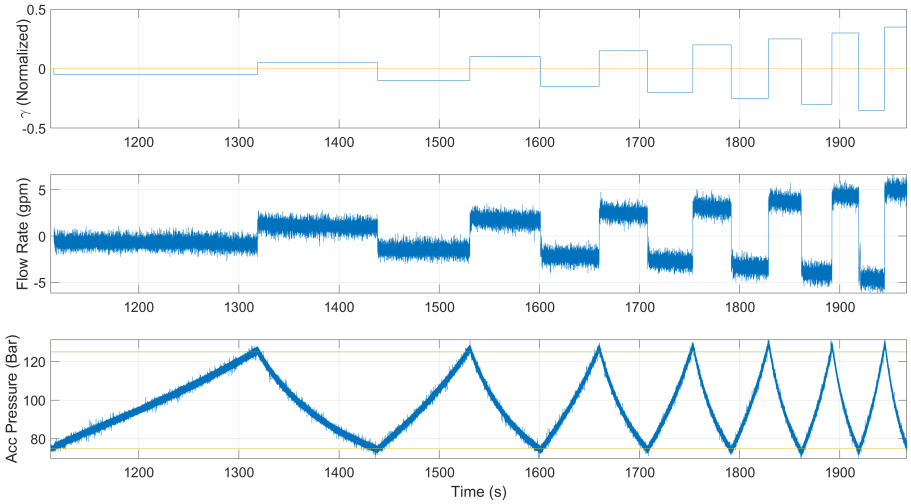

Figure 4.6: Charging and Discharging of the Accumulator

The time for the accumulator to charge from 75 to 125 bar and discharge from 125 to 75 bar was recorded for the cycles in Figure 4.6. The resulting measured flow rates were inputs for the simulation models, and results are compared. Table 4.1 shows the input flow rate compared to the resulting time to charge or discharge 50 bar in experimentation and simulation.

Table 4.1: Seconds to Charge/Discharge

Swash Angle	-.05	.05	-.1	.1	-.15	.15	-.2	.2	-.25	.25	-.3	-.35	.35
Flow Rate(gpm)	0.7	1.1	1.5	1.8	2.2	2.4	2.7	3.1	3.3	3.7	4.0	4.7	5.1
Experiment	205	115	89	66	56	46	42	35	32	29	27	23	21
Adiabatic	158	98	71	59	48	43	39	34	31	28	27	22	21
Heat Transfer	211	117	93	68	57	47	42	36	32	28	27	23	21
Isothermal	321	199	145	121	97	88	78	69	64	58	52	45	42

Table 4.1 shows that at higher flow rates the response time for the experimental system is adiabatic. The heat transfer model also matches well with experimental results, and acts adiabatic. As the flow rate decreases, the time to charge the real accumulator drifts away from the adiabatic model and closer to the isothermal model. The heat transfer results also drift from the adiabatic model towards the isothermal model. The heat transfer model stays near the experimental results at all flow rates. Even at low flow rates, the isothermal result does not match with how the accumulator reacts. The heat transfer model will work at all flow rates, yet is only needed for lower flow rates. The adiabatic assumption is equally valid for flow rates over 4 gpm.

4.2.3 Accumulator Losses to Pump Cooling

In Figure 4.6 and Table 4.1, equal displacements in positive and negative directions do not correlate to equal flow rates, although they are running at the same rotor speed. The flow rate plot appears biased to measure a higher flow during discharging than charging.

After consultation with industry, it was determined that the bias is caused by internal cooling flow in the secondary pump. The secondary pump needs to steal some flow in order to properly cool and lubricate the internal bearings. It does this with built in orifices. Typically, this flow would be provided by the low pressure port. In this non-standard application, the low pressure port is at atmospheric pressure, so no flow is forced through these orifices. The flow is taken from wherever possible. To quantify

this lost flow rate, experiments were performed.

To quantify said losses when the swash plate is centered, and the ESS is inactive, the accumulator was brought to several pressures and the swash plate was centered. At zero displacement, the flow temperature measurement is too clouded by noise to be reliable. Instead, the time for the accumulator to drop 10 bar in pressure was measured. By measuring two pressures, the adiabatic equation 2.4 was used to calculate the change in volume. The corresponding change in volume over the measured time gives the resulting flow rate. These results are shown in Table 4.2.

Table 4.2: Discharging rates at centered swash plate

Initial Pressure (bar)	75	100	125
Time to lose 10 bar (s)	227	129	90
Corresponding flow rate (gpm)	0.237	0.245	0.229

The measured loss flow rate is nearly constant. Each sample in the table is the average of three samples at the same initial pressure. This results in an overall average flow rate lost with zero displacement of 0.237 gpm.

The flow sensor measures the flow between the secondary pump and the accumulator. There is a flow for charging and discharging of the accumulator, and a flow caused by the need for cooling flow. When charging, flow is forced into the accumulator. No flow is lost to cooling. When discharging, the accumulator supplies flow for powering the secondary pump, but also supplies flow for cooling. This increases the system losses.

Table 4.5 highlights the theoretical flow rate as compared to the actual flow rate for

a number of data points.

Table 4.3: Quantifying accumulator losses

Swash Angle	-.15	.15	-.2	.2	-.25	.25	-.35	.35
Flow Rate(gpm)	2.19	2.42	2.73	3.07	3.32	3.71	4.65	5.09
Theoretical (gpm)	2.01	2.01	2.69	2.69	3.35	3.35	4.7	4.70
Difference (gpm)	.184	.412	.0326	.3828	-.0283	.3600	-.0463	.3550

The theoretical flow rate is the displacement multiplied by the rotor speed. When charging, the flow rate is approximately equal to the theoretical flow rate. This is because there are no cooling losses while charging.

When discharging, the flow rate is notably higher than theoretical. This is because the flow sensor is reading both the flow displaced by the secondary pump, and the leakage flow taken from the high pressure accumulator. By taking the average, the dischargng leakage flow is found to be around 0.377 gpm. The resulting cooling flow leakage strategy is added to the simulation, and summarized in table 4.4

Table 4.4: Accumulator Losses in Simulation

Action	Charging	Inactive	Discharging
Simulated Flow Losses (gpm)	0	0.237	0.377

These losses are significant and undesirable. By adding a directional valve between the accumulator and secondary pump, flow is allowed into the accumulator always, but only out of the accumulator when a signal is sent. This could be used to optimally

regulate both temperature of the secondary pump and minimize losses.

The characterization of the accumulator and its losses are vital for improving the accuracy of the simulation. The losses caused by heat transfer and friction in the accumulator, losses caused by cooling of the secondary pump, and losses caused by turning of the ESS are added to the simulation to increase the model fidelity. With a more accurate simulation model, experiments are performed and compared to simulations for the hybrid system. This is done with step and turbulent wind inputs.

4.3 Step Wind

Using the knowledge from the accumulator characterization, the simulation is tuned to match the real characteristics of the accumulator. The precharge pressure is increased from the characterization experiments to 100 bar, and the heat transfer model is adjusted accordingly. Step input wind is given to the hybrid system and its performance is shown in Figure 4.7 . The maximum accumulator pressure for the controller is set to 200 bar. Experimental results for HST pressure and rotor speed are filtered with a low-pass filter to minimize noise caused by test bed vibrations.

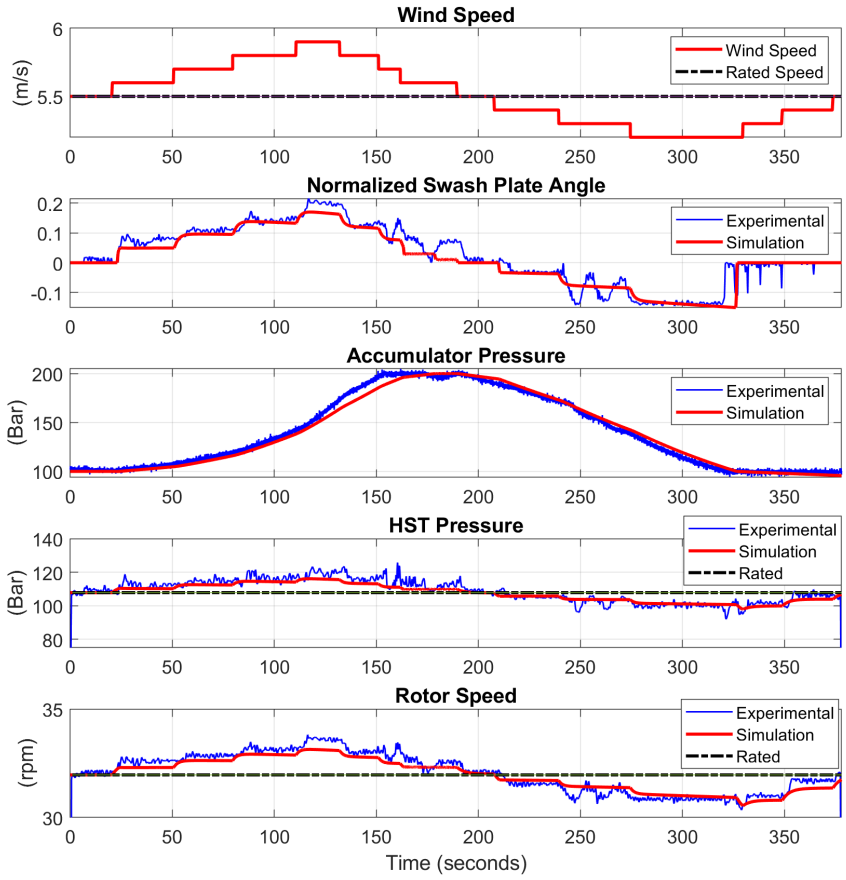

Figure 4.7: Step Wind Results

The experimental performance of the hybrid transmission matches closely with the tuned simulation. From 0 to 125 seconds, the wind speed is increasing in small step increments above the rated wind speed. The HST pressure is above rated, and the accumulator is not full. The turbine is in mode III and the accumulator begins to charge. Power is actively removed from the HST. The heat transfer accumulator model accurately predicts the performance of the accumulator. The experimental results are

noisy and cause some variation in the swash plate angle, however the average of the two is similar. HST power in the simulation and the experiment are similar.

From 125 to 175 seconds the wind speed is decreasing in step increments, but is still above the rated wind speed. The HST pressure is above the rated pressure and at 150 seconds the accumulator is full. The turbine is in mode IV and artificial blade pitch control is activated. Both controllers work by maintaining the accumulator at the maximum pressure. In the simulation, the blade pitch control limits the input torque to the rated torque over a period of 10 seconds. The rotor speed and HST torque return to the rated power. In the experiment, the same blade pitch control is implemented, and the HST pressure and rotor speed results return to the rated power. However, the implementation of blade pitch control in the test platform is not as smooth. Due to the coupled control system in the test platform, when the platform attempts to lower input torque rapidly, there is a brief sinusoidal response in HST pressure and rotor speed. This causes the HST power to fluctuate in mode IV.

From 200 to 325 seconds the wind speed is decreasing below the rated speed in step increments. The HST pressure is below rated, and the accumulator is not empty. The system is in mode II, and power is being added to the HST. The accumulator pressure, swash plate angle, HST pressure, and rotor speed match in simulation and experimentation. Due to a rapid drop in test platform power at 250 seconds, there are some sinusoidal variations in HST power.

At 325 seconds, the accumulator fully discharges. The HST pressure is below rated,

and the accumulator is empty. The system is in mode I, and the ESS is inactive. The simulation accumulator is empty slightly after the experimental accumulator, causing the slight difference in the swash plate angle. The system acts as a non-hybrid system, and the experiment and simulation match.

Mode V operation is designed to make the transition to other control modes smoother. The system is in mode V at 0 and 200 seconds. This does not significantly affect the results, but prevents fast switching between control regions.

One goal of the ESS is to maintain the HST near the rated power. Figure 4.7 is repeated and overlaid with non-hybrid simulation without blade pitch results in Figure 4.8.

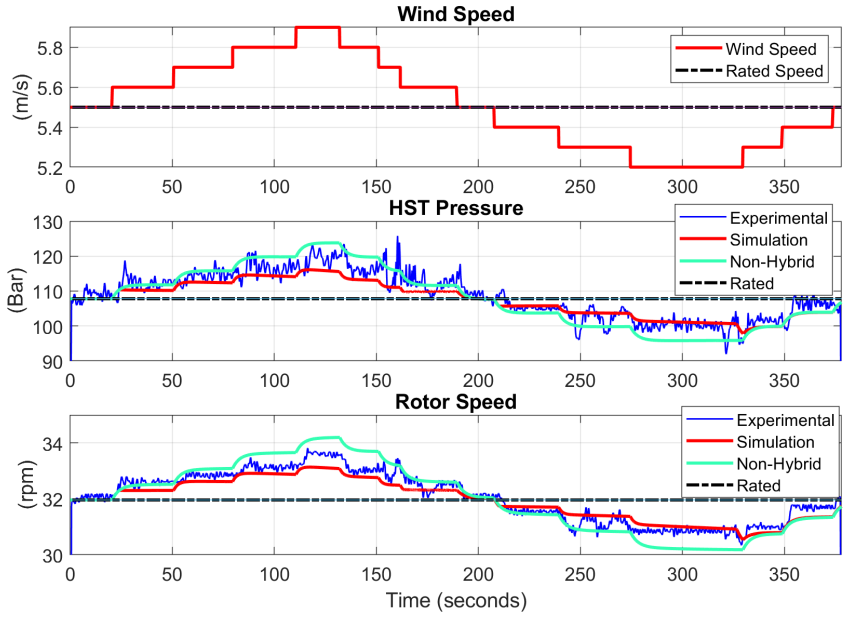

Figure 4.8: Step Wind Results with Non-Hybrid System

Before 50 seconds, the hybrid system simulation is only removing a small amount of energy, and results are similar to the non-hybrid system simulation and experimental results. As the wind speed increases, the difference becomes more apparent. The hybrid simulation and experiments show a HST pressure and rotor speed significantly closer to the rated pressure and speed than the non-hybrid system. This is evidence of the hybrid system working effectively to remove power from the HST to keep the HST at a smoother power level.

After 200 seconds, the accumulator is discharging. The ESS is able to supply power to the HST to keep its power closer to the rated power in the simulation and experiment. At 325 seconds, when the accumulator is empty, the hybrid and non-hybrid systems act the same, as no more power can be used to supply the HST.

Power is being removed and added to the HST, but it is not being removed and added quickly enough to maintain a constant operation at the rated power. This is because of the controller. The proportional controller is stable for a limited range of gains, as discussed in Appendix A. In the linearized controller design system, the maximum stable gain is sufficient for maintaining the HST at near constant operation at the rated power. Since the real system is highly nonlinear, the real maximum stable gain is lower than predicted. The lower gain results in a slower response to removing and adding energy to the HST. If the rate at which power can be added and removed from the HST is increased, the system will operate even smoother than currently.

Wind step results show the effectiveness of the energy storage system, however they

are not realistic. To accurately test how effective the hybrid system is in a real application, realistic wind is generated and the system is experimentally tested.

4.4 Turbulent Wind

Wind data was generated by NREL FAST code. This is a National Renewable Energy Lab approved code for generating wind samples with a given average wind speed and turbulence intensity [36]. The results of the hybrid system under this realistic wind are compared to the simulation in Figure 4.9.

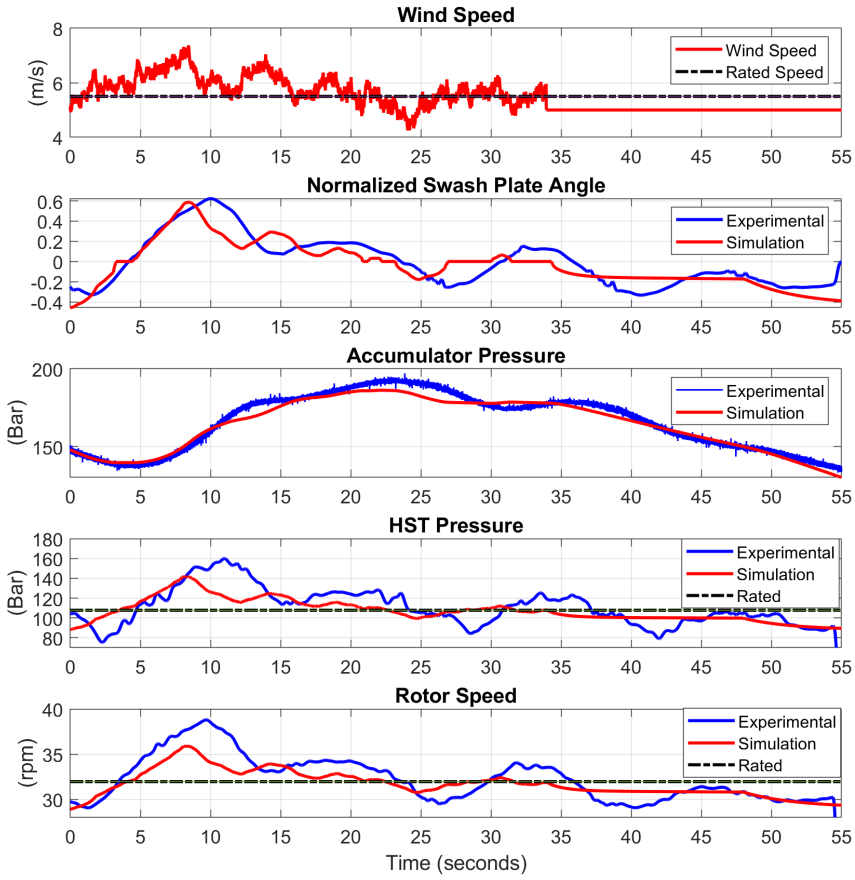

Figure 4.9: Turbulent Wind Results

Similar to step wind, the HST pressure and rotor speed measurements are filtered with a low-pass filter. Before 10 seconds, the wind speed is rapidly fluctuating above the rated wind speed. The accumulator begins to charge, and the simulation and experiment match well. From 10 seconds onward, the wind fluctuates on a much larger scale. The simulation and experimental results diverge. The large-scale changes in wind speed, and the coupled controller of the test bed cause sinusoidal fluctuations in the HST

pressure and rotor speed. The simulation results are almost exactly at the average of the experimental results, with the experimental HST power fluctuating above and below the simulated HST power. Although this fluctuation is not ideal, the simulation results still accurately average the real results, even though the unmodeled dynamics of the coupled test platform controller causes these oscillations in experimental results. These coupled platform dynamics will not appear in a real system, and the simulation can still be used for estimation.

To quantify the amount of additional energy produced with the hybrid system, the simulation that has been experimentally validated with step and turbulent experiments was compared to a non-hybrid simulation with blade pitch control. By integrating the output power of the HST for the hybrid and non-hybrid systems, the total amount of energy produced is calculated. All power above the HST rated power is not counted and is assumed to be negated with instantaneous blade pitch for both hybrid and non-hybrid systems. With this method, the simulation results from Figure 4.9 produce an additional 1% energy than the non-hybrid system.

This sample of wind is not indicative of the whole turbine performance. More information is needed to quantify the benefits of the hybrid system. The most relevant parameter is the additional energy produced on a yearly basis. The methods and results for calculating the annual energy production are discussed in the next section.

4.5 Annual Energy Production

Wind speeds vary on a yearly, monthly, daily, and hourly basis, as shown in Figure 1.6. The Bin Method is a common method for wind turbine manufacturers and engineers to estimate the amount of energy a turbine can produce on a yearly basis. Typically, an engineer will record months to years of data for a particular location and create a histogram of the wind speed to determine the percent of time the wind is withing certain ranges, or "bins" of speed. The amount of energy a turbine can produce within these bins is multiplied by the amount of time the wind speed is in that bin on a yearly basis. The sum gives the annual energy production. When wind data is not available, a statistical Weibull distribution can be used for this estimation. For small to midsize turbines, it is common practice to approximate the Weibull distribution as a Rayleigh distribution [10].

The Rayleigh distribution is completely determined by an average wind speed. The 60kW Polaris turbine used in this thesis is designed for IEC class II wind, with an average wind speed of 8.5 m/s. This distribution is plotted from 0 to 30 m/s wind speed, overlaid with 30 bins in figure 4.10

For each bin, NREL Turbsim was used to produce wind samples with a NREL "normal turbulence model" and an average wind speed [36]. For each bin, a 1-hr sample wind simulation with the bins average wind speed was produced. A simulation of the hybrid system as compared to a non-hybrid system was run for each wind sample. The amount of additional energy produced by the hybrid system was recorded for each bin.

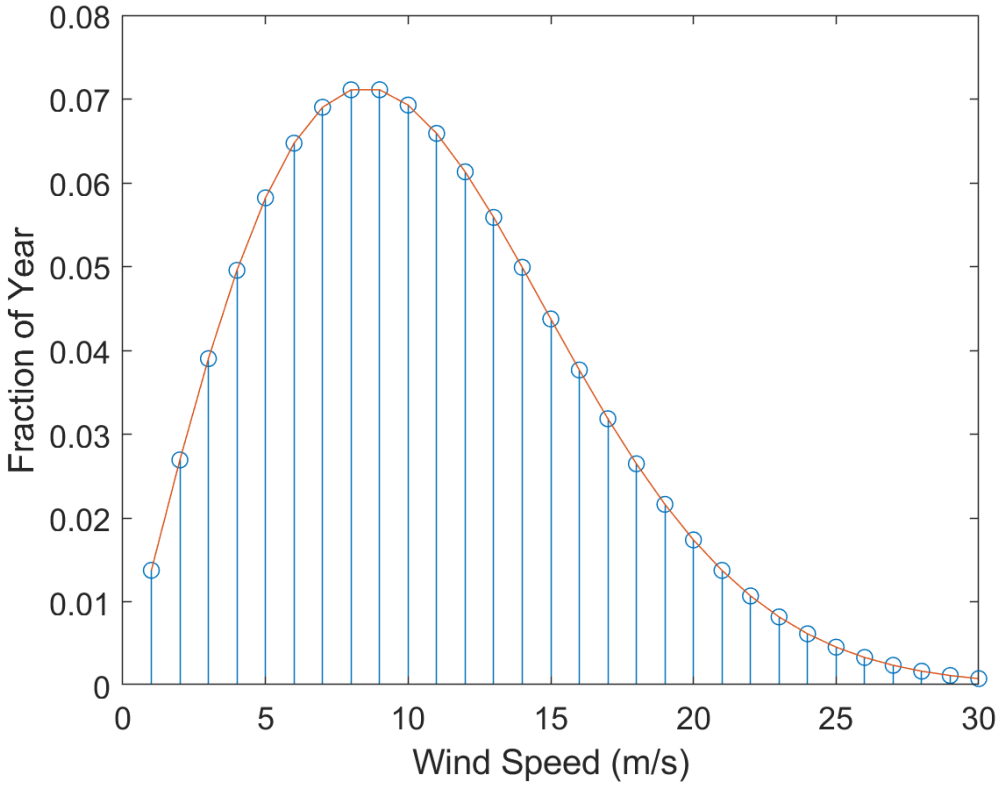

Figure 4.10: Rayleigh Wind Speed Distribution for IEC Class II Wind

The weighted sum was taken to get the additional annual energy production.

The losses due to secondary pump cooling and additional turning losses of the hybrid system have been quantified. Turning losses can be mostly negated with a clutch, and secondary pump cooling losses can be mostly negated with a directional valve. To analyze how important these components are, they were both artificially added to the simulation.

The clutch is added in the simulation by setting the turning losses (charge pump

static losses and increased damping) to zero when the system is in mode I. The directional valve is added in the simulation by setting the loss flow rate out of the accumulator to zero when the accumulator is charging or inactive. When discharging, these losses cannot be negated by the valve. Accumulator losses quantified in the heat transfer model cannot be negated. Table 4.5 summarizes the loss parameters and the four cases, and how they are implemented in the five modes of the Rule-Based Control Scheme.

Table 4.5: Operating Cases of Losses in Simulation

Case	Cooling Losses	Charge Pump Losses	Increased Damping Coefficient
No Valve or Clutch	All modes	All modes	All modes
Valve Only	Mode II	All modes	All modes
Clutch Only	Modes II,III,IV,V	Mode II,III,IV,V	Mode II,III,IV,V
Valve and Clutch	Mode II	Mode II,III,IV,V	Mode II,III,IV,V

The most significant benefit of the clutch is that it negates nearly all loses at low wind speeds. The directional valve negates losses for cooling for all modes except while discharging. The simulations were performed for each bin with and without the clutch and directional valve. The amount of additional energy produced was recorded, and using the bin method, the annual energy production was produced. The results for annual energy production are shown in table 4.6.

Table 4.6: Percent of Additional Annual Energy Produced

No Valve or Clutch	Valve Only	Clutch Only	Valve and Clutch
1.91	1.92	3.49	3.52

The system with the valve and the clutch produced an additional 3.5% additional annual energy. Without the clutch or directional valve, this value is reduced to 1.9%. The clutch appears to have a significantly higher impact than the valve.

The clutch removes a significant amount of losses when the ESS is inactive. In wind speeds near the rated speed, the clutch is always active, and the losses reduce the amount of energy stored. In wind speeds higher than the rated speed, the clutch is active, and there are increased losses in the system, but due to the flexibility of blade pitch control, the system can pitch blades less sharply to make up for those losses. The hybrid and non-hybrid systems produce the same amount of energy. There is a significant amount of time where the wind speeds are lower than rated. In these cases, the clutch is inactive, and additional losses are negated. Without a clutch, these losses

make the turbine produce less energy. In low speed winds, the hybrid system without a clutch will produce less energy than a non-hybrid system. However, without a clutch, the net is still additional energy production. This indicated that the clutch is an essential part of the hybrid system for increased performance.

Meanwhile, the valve removes losses only when the accumulator is inactive. In wind samples near the rated speed, the accumulator is constantly charging and discharging, leaving minimal time for the accumulator to be inactive, meaning the valve has no significant impact. In wind samples above the rated speed, blade pitch control can make up the losses of the accumulator, with or without the valve, similarly to the clutch. There is a significant amount of time where the wind speeds are lower than rated. In these situations, having the valve keeps the accumulator pressure constant. However, if there is no valve, the pressure will decrease. However, the accumulator has a limited amount of fluid, and the pressure can only decrease so much. This limits the amount of lost energy from the accumulator. This is why the results for including the directional valve are only slightly higher than those without the valve.

However, the valve is also important for other reasons and must be included in the hybrid system. When the accumulator pressure drops to values below the precharge pressure and then re-charges, the bladder can be damaged over time, leading to decreased reliability. If a clutch is included in the system, the valve is required to block off the accumulator flow when inactive. Even at low pressure, the accumulator is storing energy, and if the shaft is decoupled, quick release of accumulator power can cause rapid

loading on the gearbox, which can lead to premature failure. These releases are also uncontrolled and can potentially damage other components. Therefore, the optimal design includes a clutch and valve.

Chapter 5

Conclusions and Future Work

5.1 Conclusion

The earth is in a climate crisis, and renewable energy sources are the best way to avoid detrimental long-term effects to the planet. Most research is focused on utility scale turbines, but there is a need for mid-sized turbines. These turbines need improved reliability and power generation capabilities. The first step to improvement is using a HST instead of a conventional gearbox transmission. The next step is to hybridize the system.

Hybridization of a wind turbine transmission by adding a hydraulic ESS is a high-power solution for a high-power application. A gearbox, secondary pump, and accumulator are added to remove and add energy to the HST when wind speeds are above or below rated. This maintains a smooth transmission power output, and increases the

system reliability.

The system was dynamically modeled, and a rule-based control scheme was developed to operate the hybrid system. Negative proportional gain was selected and verified to using a stable control strategy. Preliminary simulation was used to select hardware for the upgrade of the test platform.

The test platform was upgraded to include accumulator characterization and hybrid system testing with an ESS on an independent circuit. The ESS was experimentally characterized and used to improve the fidelity of the simulation. The simulation was then tested against experimental data and validated.

The simulation was then expanded to an annual wind energy study, in which the total amount of energy produced was calculated. The simulation was modified to explore the results if a clutch and directional valve were added to the system to minimize losses.

It was found that the hybrid system with a clutch and directional valve added produces an additional 3.5% energy on a yearly basis. The hybrid system also smooths out the output power when compared to a non-hybrid HST, improving energy quality and transmission reliability. The system is significantly faster than blade pitch control, and due to its high power, it can quickly remove and add energy to the system. The high power of the accumulator can also provide ancillary benefits, such as fault ride-through, and severe weather yaw and pitch control.

Although the hybrid system has shown its benefits, it is a first-round proof of concept design. There is room for improvement in future research.

5.2 Future Research

The results show that the system generates more power and is likely more reliable than a non-hybrid system, with a smoother output to the grid. However, the control strategy and design of the hybrid system is not optimized. There is room for improvement in the hybrid system.

5.2.1 Improving Control Strategies

The current control strategy is a simple rule-based control with a few modifications. It is likely that this is not the optimal control strategy. It also has a limited range of stable gains that limits the performance of the hybrid system. It is evident that an improved control strategy is needed to operate the system for better performance. Research into a new, improved control strategy is underway.

5.2.2 Advanced Control Strategies

Further research on optimizing hybrid system performance in regions 2 and 3 is a future plan. Advanced control strategies such as extremum-seeking control and model predictive control can also optimize the amount of energy captured in regions 2 and 3. These control strategies could significantly improve the amount of energy captured by the hybrid system without sacrificing reliability. Research into these strategies is currently underway.

5.2.3 Detailed Cost Analysis

The Levelized Cost Of Electricity (LCOE) is a benchmark used to quantify the true price to produce electricity over its lifetime. This includes start-up and maintenance costs, as well as system reliability and benefits. By comparing the LCOE with and without the clutch and valve, more accurate decisions can be made on whether to include the components in the ESS. This is a complicated project, outside of the scope of this thesis.

5.2.4 Pitch and Yaw Control

Even with the hybrid system, blade pitch control and yaw control are needed. In a traditional turbine these are controlled by independent hydraulic actuators. These devices can use a lot of energy to power. However, the energy stored in the accumulator is high power, and is sufficient to power both pitch and yaw control. Pitch control with the hybrid system is only necessary when in mode IV, in which the accumulator is fully charged, and could be used to power blade-pitch with additional valving and control strategies. This could save on both cost and energy. Yaw control is needed to always face the turbine in the correct wind direction. This is typically actively done, and could be powered either by stored energy in the accumulator or HST power. Initial research on simulating the benefit and cost of both of these ideas is underway.

5.2.5 Holistic Hydraulic System

Currently, the ESS runs on an independent hydraulic circuit. Eventually, an optimized system would include an optimized control that uses one hydraulic circuit for the HST, ESS, and blade pitch and yaw control. This idea is far away, but could significantly lower the cost and improve efficiency if implemented.

References

[1] S. Arrhenius. On the influence of carbonic acid in the air upon the temperature of the ground. *Philosophical Magazine and Journal of Science*, 41(251):237–276, 1896.

[2] The White House. Restoring the quality of our environment. *Philosophical Magazine and Journal of Science*, 1965.

[3] G. Marland T. Boden and R. Andres. Global, regional, and national fossil-fuel co2 emissions. *Carbon Dioxide Information Analysis Center, Oak Ridge National Laboratory*, u.s. department of energy, 2017.

[4] Summary for policymakers, in climate change 2007: Impacts, adaptation and vulnerability. *Contribution of Working Group II to the Fourth Assessment Report of the Intergovernmental Panel on Climate Change*, page 17, 2007.

[5] Summary for policymakers. in: Global warming of 1.5c. an ipcc special report on the impacts of global warming of 1.5c above pre-industrial levels and related global

greenhouse gas emission pathways, in the context of strengthening the global response to the threat of climate change, sustainable development, and efforts to eradicate poverty. *World Meteorological Organization, Geneva, Switzerland*, page 32, 2007.

[6] Paris agreement to the united nations framework convention on climate change. *United Nations Framework Convention on Climate Change*, pages 16–1104, Dec 2015.

[7] Department of Energy. International energy outlook 2019. *US Energy information administration*, 2019.

[8] Wind Vision Report Department of Energy, United States .

[9] T. Ackermann. R. Leutz. and J. Hobohm. Worldwide offshore wind potential and european projects. *Power Engineering Society Summer Meeting*, pages 4–9, 2001.

[10] Future of wind: Deployment, investment, technology, grid integration and socio-economic aspects. Technical report, International Renewable Energy Agency, 2019.

[11] 2018 distributed wind market report. Technical report, United States Department of Energy, 2018.

[12] S. Sheng. Report on wind turbine subsystem reliability - a survey of various databases. *National renewable energy laboratory-NREL/PR-5000-59111*, 2013.

[13] J. Schmitz. N. Vatheuer. and H. Murrenhoff. Hydrostatic drive train in wind energy plants. *RWTH Aachen University, IFAS Aachen, Germany*, 2011.

[14] C. Ai. G. Wei. Q. Hu. Y. Zhang. L. Chen. G. Jiawei. and H. Zengrui. Application of the Feedback Linearization in Maximum Power Point Tracking Control for Hydraulic Wind Turbine. *Energies*, 13(6):1529, 2020.

[15] K. Johnson. L. Pao. M. Balas. and J. Lee. Control of variable-speed wind turbines: Standard and adaptive techniques for maximizing energy capture. *IEEE Control Systems*, 26, no. 3:70–81, 2006.

[16] Y. Xiao. Y. Li. M. Rotea. Experimental evaluation of extremum seeking based region-2 controller for cart3 wind turbine. *34th wind energy symposium*, 2016.

[17] I. Van der Hoven. Power spectrum of horizontal wind speed in the frequency range from 0.0007 to 900 cycles per hour. *Atmos. Sci., 14, pp*, pages 160–164, 1957.

[18] J. Van de Ven. M. Olson. P. Li. Development of a hydro-mechanical hydraulic hybrid drive train with independent wheel torque control for an urban passenger vehicle. *National Conference on Fluid Power*, page 503, 2008.

[19] H. Kwonab. M. Ivantysynovaa. Experimental and theoretical studies on energy characteristics of hydraulic hybrids for thermal management. *Energy Vol 223*, 2021.

[20] F. Díaz-González. A. Sumper. O. Gomis-Bellmunt. and R. Villafáfila-Robles. A Review of Energy Storage Technologies for Wind Power Applications. *Renewable and sustainable energy reviews*, 16(4):2154–2171, 2012.

[21] L. Wei. Z. Liu. Y. Zhao G. Wang. and Y. Tao. Modeling and Control of a 600 kW Closed Hydraulic Wind Turbine with an Energy Storage System. *Applied Sciences*, 8(8):1314, 2018.

[22] R. Dutta. F. Wang. B. Bohlman. and K. Stelson. Analysis of Short-term Energy Storage for Midsize Hydrostatic Wind Turbine. *Journal of Dynamic Systems, Measurement, and Control*, 136(1):011007, 2014.

[23] B. Mohanty. S. Dhople. and K. Stelson. A dynamical model for a hydrostatic wind turbine transmission coupled to the grid with a synchronous generator. *2019 American Control Conference (ACC)*, pages 5774–5779, 2019.

[24] B. Mohanty. F. Wang. and K. Stelson. Design of a Power Regenerative Hydrostatic Wind Turbine Test Platform. *JFPS International Journal of Fluid Power System*, 11(3):130–135, 2019.

[25] B. Mohanty. and K. Stelson. High Fidelity Dynamic Modelling and Control of Power Regenerative Hydrostatic Wind Turbine Test Platform. *Proceedings of the ASME BATH 2018 Symposium on Fluid Power and Motion Control*, 2018.

[26] E. Mohr. B. Mohanty and K. Stelson. Short-Term Energy Storage System for Hydraulic Hybrid Wind Turbine Transmission. *Proceedings of the ASME BATH 2020 Symposium on Fluid Power and Motion Control*, 2020.

[27] A. Pourmovahed and D. Otis. Effects of thermal damping on the dynamic response of a hydraulic motoraccumulator system. pages 21–26, 1982.

[28] A. Pourmovahed and D. Otis. "an experimental thermal time-constant correlation for hydraulic accumulators. 1986.

[29] A. Pourmovahed and D. R. Otis. "an algorithm for computing nonflow gas processes in gas springs and hydropneumatic accumulators. *Dyn. Syst. Meas, Control*, 1985.

[30] H. Paynter. E. Fahrenthold. and C. Rotz. Wall heat transfer and storage effects on the thermal dynamics of otiseffect gas compression processes. *Journal of Dynamic systems measurement and control*, pages 728–733, 1990.

[31] E. Mohr. D. Escobar. D. Ajagbe. and K. Stelson. Modeling of Hydraulic Hybrid Wind Turbine Transmission with Realistic Accumulator. *Proceedings of the International Conference on Fluid Power*, 2021.

[32] Jason H. Laks, Lucy Y. Pao, and Alan D. Wright. Control of Wind Turbines: Past, Present, and Future. *American Control Conference 2009. ACC '09., pp. 2096-2103,2009*, 2009.

[33] B. Mohanty. and K. Stelson. Characterization and calibration of a power regenerative hydrostatic wind turbine test bed using an advanced control valve. *11th international Fluid Power Conference*, 2018.

[34] Accumulator Sizing Guide. Technical report, Hydac, Inc, 2015.

[35] Accumulator Detailed Report. Technical report, Hydraulics and Pneumatics, 2016.

[36] J. Jonkman. M. Jason. J. Buhl. and L. Marshall. Fast User's Guide – Updated August 2005. Technical report, National Renewable Energy Lab.(NREL), Golden, CO (United States), 2005.

[37] HMV-02 Product Manual. Technical report, Linde Hydraulics, 2016.

Appendix A

Controller Stability Validation

The hybrid system is a nonlinear, 3-dimensional MIMO system, meaning there are 3 inputs and 3 states. The system was linearized about the rated wind speed of the turbine and the precharge pressure of the accumulator. The open loop poles of the system are stable, but the zeros for each of the 9 transfer functions between inputs and outputs were analyzed to ensure stability. Of the 9, there was an unstable relation between the secondary swash plate angle and the accumulator pressure. The root locus of this transfer function is shown in Figure A.1.

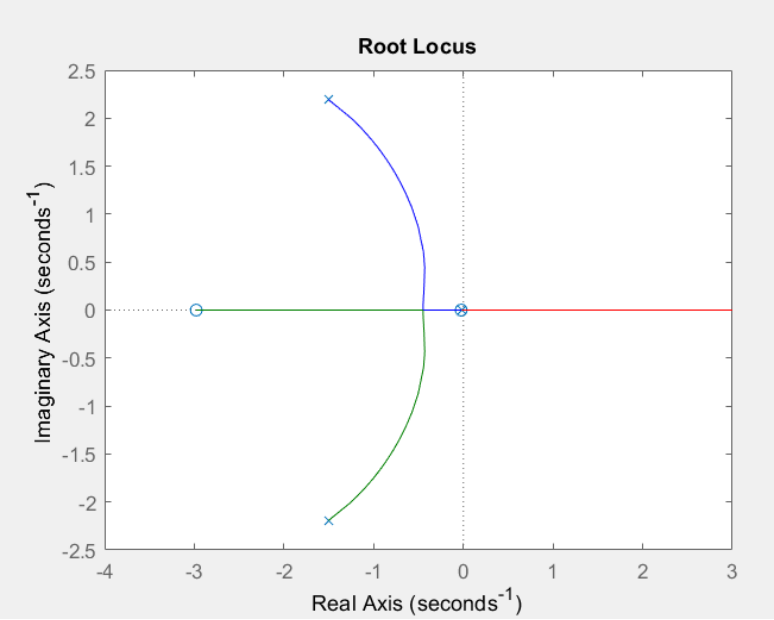

Figure A.1: Root Locus of Problematic Transfer Function

With the location of these zeros, the system is unstable with P, PI, or PID control. The zero angle transfer pole map was used to analyze system performance with a negative gain. With a negative proportional control gain, the system was found to be stable. Figure A.2 shows the Bode plot, root locus, and step response of the designed controller

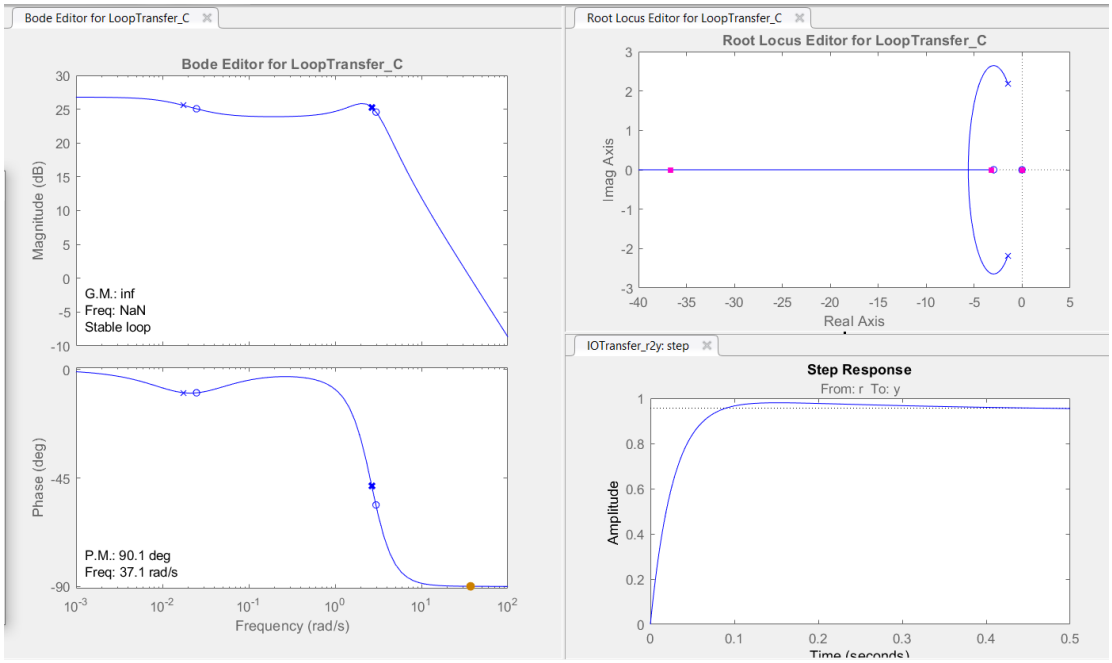

Figure A.2: Response of System with Negative Gain

The resulting root locus is stable for all proportional gains. The Bode plot indicates the controller has an infinite gain margin and a phase margin of 90 degrees, demonstrating stability. The step response shows that the system is quick, with a time constant of less than 0.1 seconds, and only has a small overshoot for the selected gain.

However, this is a MIMO system, and the other transfer functions have to be considered. With a negative proportional gain, the transfer function between the swash plate angle and the rotor speed, and the the transfer function between the swash plate angle and the HST pressure both become unstable. There is a limited window in which a negative proportional gain can be used and is stable for all transfer functions.

These results are encouraging, but control of non-linear systems can be tricky, and a

non-linear simulation and experiments must be performed to verify stability. A preliminary, non-linear simulation consisting of the system dynamics and control was produced to verify controller stability.

Appendix B

Gearbox Torque Limiting Control

The gearbox is rated for 5 kNm. Meanwhile, the torque produced on the rotor is proportional to the cube of wind speed. Figure B.1 shows preliminary simulation results for the resulting rotor torque for 60 kW turbine from steady state wind speeds for the hybrid and non-hybrid transmissions.

With a non-hybrid system, the excess power is split between the rotor speed and torque. But with the hybrid system, all excess power goes to torque, as the rotor speed is controlled to be constant. All the torque above the rated torque is applied directly to the gearbox. As shown in Figure B.1, a 1 m/s increase in the wind speed above rated can apply 3 kNm to the gearbox, and a 2 m/s increase in wind speed above rated can apply 8 kNm to the gearbox. Although wind speeds will not often have this drastic of a change near the rated speed, it is important to ensure the gearbox will not be damaged. The secondary swash plate is intentionally limited in these situations by taking the

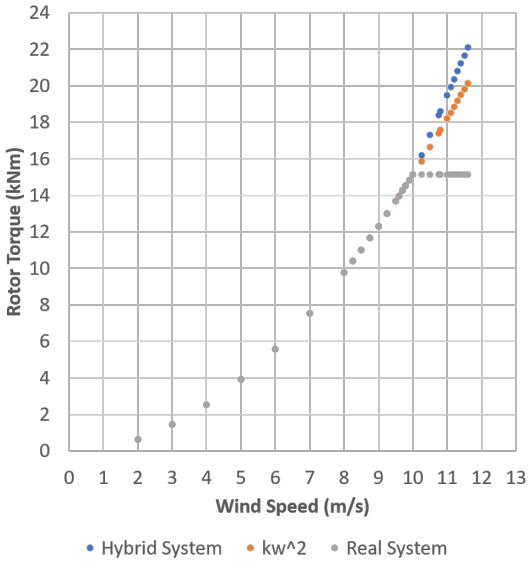

Figure B.1: Gearbox Torque vs Wind Speed

rated torque of the gearbox and actively converting to a maximum swash plate angle γ dependent on the accumulator pressure via:

$$\gamma_{limit} = \frac{\tau_{limit}}{G_r D_{p2} P_{Acc}} \tag{B.1}$$

The limiting torque is set to 5 kNm and the accumulator pressure is actively measured. This creates a constantly updating maximum allowable swash plate angle which is implemented as a saturation. This ensures that quick bursts of extra power will not damage the energy storage system, but will instead add this additional power to the HST where a pressure relief valve set to just above rated pressure will minimize damage.

Appendix C

ESS Shaft Design

In the previous test bed setup, the low speed shaft consisted of two bearings and two identical motors as shown in figure C.1.

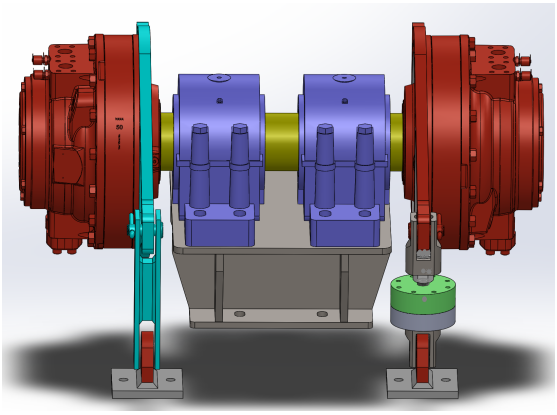

Figure C.1: HST Platform Low Speed Shaft - Before

The motors use torque arms for a cheaper method of torque measurement. They are in a perfect balance due to symmetry. Once the ESS is added, a force analysis was done to ensure there was no shaft imbalance, misalignment, or over-constraint. Multiple

designs were discussed, including using a third torque arm on the gearbox instead of a torque sensor and directly mounting the pump to the gearbox, mounting the gearbox and pump to one mounting plate, or using the selected design of two separate mounting plates and a torque sensor. The selected design can be seen in figure C.2.

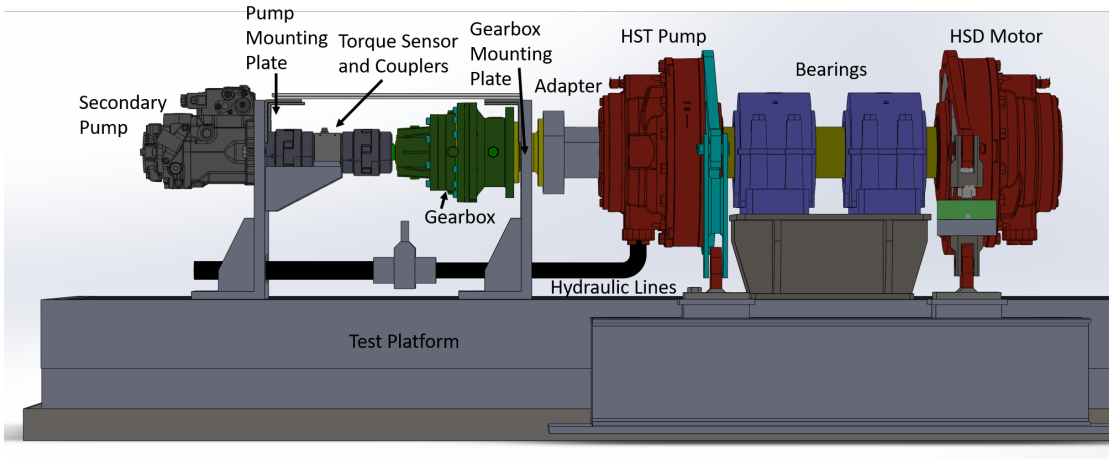

Figure C.2: Energy Storage System Shaft

This option was selected because of its simplistic and robust design. However, it required design and manufacturing of two mounting plates, a torque sensor mount, and an adapter to the HST Pump.

Appendix D

Special Component Designs

Mounting Plates and FEA

The mounting plates are designed to support the weight and bending moment of the other components along the shaft, without overconstraining or causing shaft misalignment. These plates must also withstand the high torque from operation of the test bed, and have a large hole in order to allow hydraulic lines to pass through, while holding the gearbox and secondary pump. The specialty designed plates are shown in Figure D.1.

Finite Element Analysis (FEA) was used to verify in simulation that the mounting plates were sufficiently designed, as shown in Appendix E. The designed plates had a safety factor of 16 and 2.6 for the pump plate and gearbox plate, respectively.

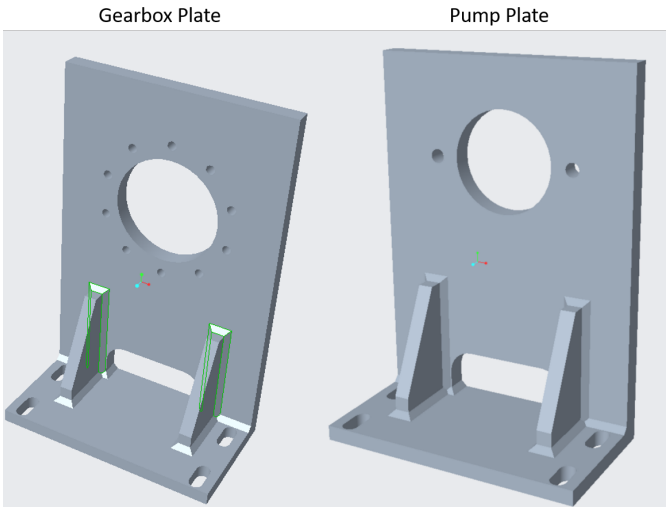

Figure D.1: Designed Mounting Plates

Low Speed Shaft Adapter

To attach the ESS to the current system a special adapter needed to be made. This adapter needed to connect the rotor shaft to the gearbox shaft through the HST motor. In a commercial application, this Hagglunds motor has common designs to use a through shaft which can connect to another motor or brake. This unit, however, was not originally designed with a through shaft, so a custom adapter was needed. The previous shaft is in contact with the entirety of the internal spline of the motor. The shaft was shortened to only use half of the internal spline. The adapter then uses the other half of the internal spline, and is hollow to be bolted to the modified shaft. This way, the torque is transmitted to the gearbox shaft safely through the motor and its internal spline. The other end of the adapter is specially made to fit a mounting flange option for the gearbox. Figure D.2 shows a cross-section of the adapter in place.

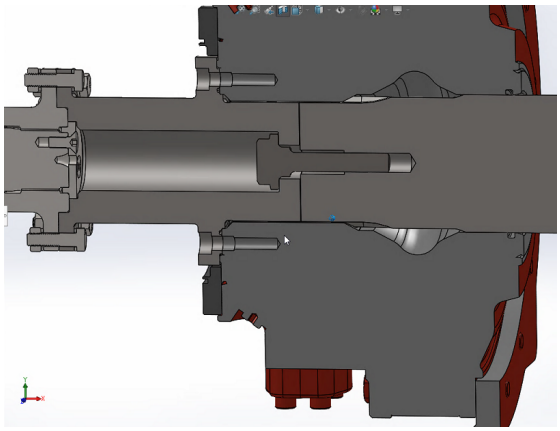

Figure D.2: Cut view of adapter

This image shows how the adapter connects the rotor shaft to the gearbox shaft. To do this, the previous shaft was cut short, and a hole was drilled to hold the bolt. Modification of the previous shaft required complete shaft removal and disassembly of the low speed shaft. In this process the large bearings used were cleaned, re-toleranced, and re-greased to ensure efficient operation.

Torque Sensor Mount and Couplers

The mounting plate for the secondary pump has a specially designed, built-in, torque sensor mount. This mount is shown in figure D.3 and is adjustable via machined slots.

This design allows for easy assembly and disassembly of the couplers required to attach the torque sensor. The gearbox is limited to 5 kNm, meaning the high speed shaft of the gearbox is limited to 160 Nm. The couplers are standard jaw type 200 Nm couplers.

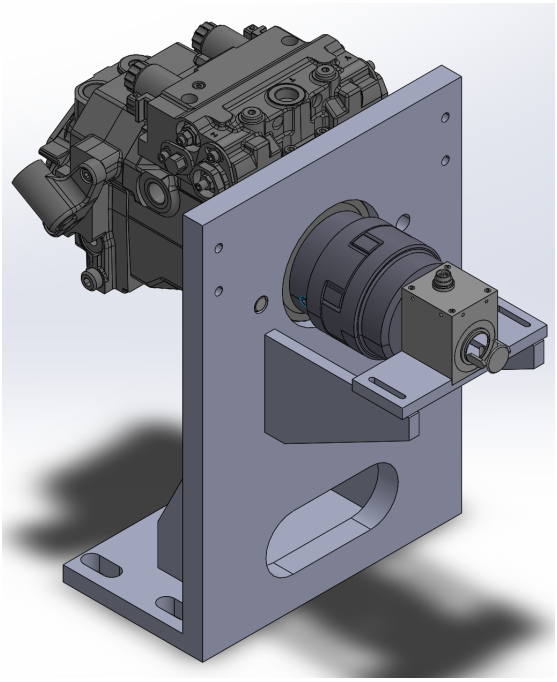

Figure D.3: Torque Sensor Mount

Appendix E

Mounting Plate FEA

Loads were determined by a force balance on the shaft of the design, and the simulated maximum torque at the gearbox. It was during these force balances that the best design for the layout was chosen. Figure E.1 Shows the results for equivalent stress on each mounting plate.

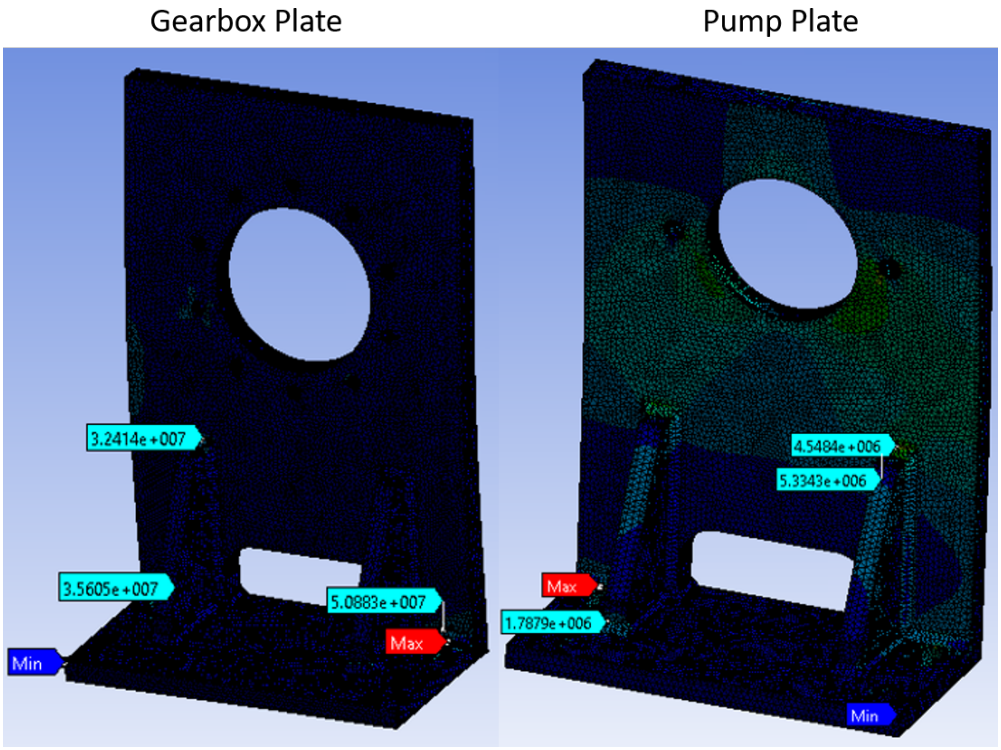

Figure E.1: Designed Mounting Plates FEA

When assuming the strength at the weld is approximately 40% of the yield strength of the steel plates, and adding an additional 10% to the maximum stress due to potential FEA solver uncertainty, The secondary pump mounting plate has a safety factor of 16, and the gearbox mounting plate had a safety factor of 2.6 at worst case loading conditions. This ensures that the plates are strong.

Appendix F

Hydraulic Circuit

The hydraulic schematic for the ESS is shown in Figure F.1.

The hydraulics are designed to run on an independent loop, such that the ESS can be added to any transmission. When charging flow runs from the tank through the P port, through the pump, through the sensor array, and into the accumulator safety valve and accumulator.

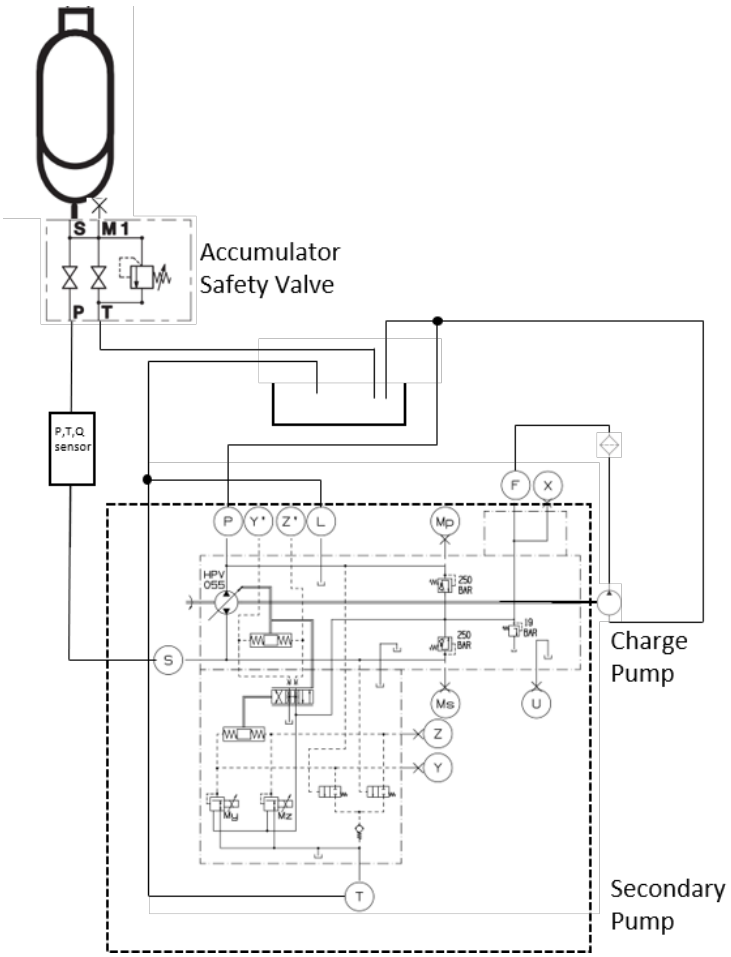

Figure F.1: Hydraulic Schematic

Appendix G

Potential Concerns

Cavitation Concerns

The selected secondary pump is designed for closed loop operation. For an HST, this works because one port is high pressure (350 bar), and the low pressure port always has a nominal pressure (40 bar). The secondary pump however is an open-loop operation, and will draw flow from its low pressure side directly from the tank (0 bar). This leads to cavitation, a process in which entrapped air is compressed enough to cause micro-explosions, which can severely damage the pump. To avoid this, a large suction line to tank was made, and the tank was elevated. The inlet pressure was monitored during experiments, and was required to meet the pressure shown in Figure G.1 [37].

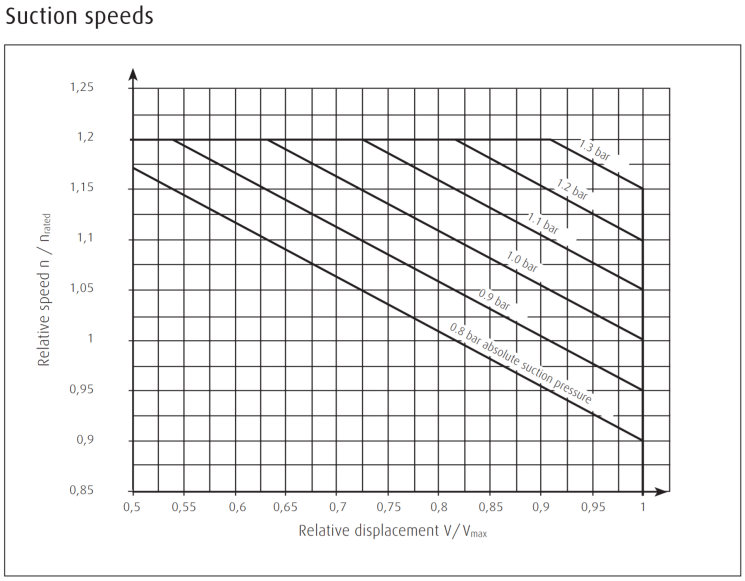

Figure G.1: Minimum Allowable Suction Pressure

Lack of Pressure Build-Up

The pump needs to build up an internal pilot pressure to power the swash plate control. The internal schematic for the secondary pump is shown in Figure G.2. Port S is connected to the accumulator, and port P is connected to the tank. There are two 350 bar system relief valves and a 19 bar charge pressure relief valve. The 350 bar valves are shown in detail in figure G.3, provided by Linde. These valves have a large spring and a small spring. When there is pressure above 350 bar on the left entrance to the valve, which is connected to the P or S port, the large spring will compress and allow flow through the bottom port, which is connected to the junction labeled with a red star. There is a loop make-up feature built in to these valves that will compress the small spring and open flow from the red star to port P or S if the pressure at the red

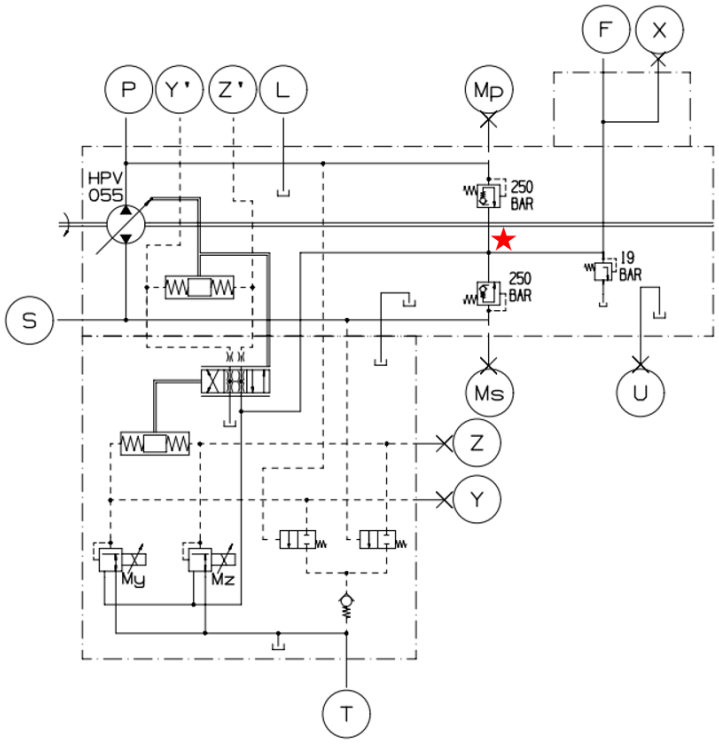

Figure G.2: Secondary Pump Diagram

star is higher. This is a measure to avoid cavatation. A 14 cc/rev charge pump is added to create flow which enters through the F port in Figure G.2. In closed-loop operation, S will always be high pressure (350 bar), and P will always be low pressure (40 bar). The 19 bar charge relief valve limits the pressure at the red star to a maximum of 19 bar, so this loop make-up function will only happen if there is an issue, and the P port has a large drop in pressure. The 19 bar at the red star is then used to power the swash plate control.

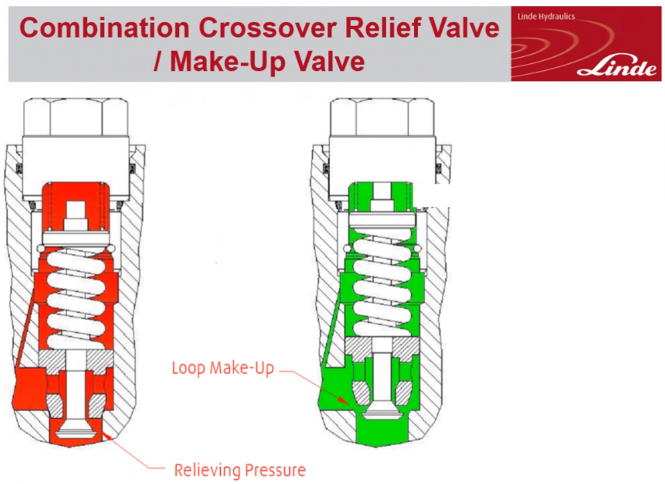

Figure G.3: System Relief Valve

Since this pump is being used in an open-loop design, the P port connected to the tank remains at around 1-5 bar, while the S port has a minimum pressure of the accumulator precharge pressure. Since the P port pressure is so low, the charge flow will activate the loop make-up function of the upper valve, which will prevent from pressure building at the red star past 6 bar, which is lower than the needed pressure to power the swash plate control. Hence, the pump will not be able to actuate its swash plate unless the loop make-up function of the upper system relief valve can be removed. To do this, the valve had to be modified in the secondary pump. This was accomplished by replacing the small spring in figure G.3 with a spring with a significantly higher spring constant. This spring will not compress unless the pressure at the red star is higher than 25 bar. Because of the 19 bar charge relief valve, the red star cannot build more than 19 bar, meaning that the function is disabled. This allows for proper pilot pressure

and swash plate control.

Appendix H

Driver

The secondary pump is controlled by two solenoids. The combination of the current delivered to each solenoid produces the swash plate angle. For single signal control of the two solenoids, a Sun Hydraulics XMD-02 driver is used. This driver is programmable to allow for a 0-5VDC signal to control two solenoids. A plot of the input signal versus the solenoid current is shown in Figure H.1

The Linde catalog indicates the required solenoid current to get the desired swash plate angle. For the 24V solenoids, a signal from 225 to 590 mA is equivalent to a signal of 0 to 100% displacement[37]. For directional flow, coild A or B must be set to a desired current, and the other coil must be set to zero current. There is a gap near 2.5V. This is done to ensure that the swash plate angle stays at zero when a 2.5 VDC signal is sent, even if there is error in the signal voltage.

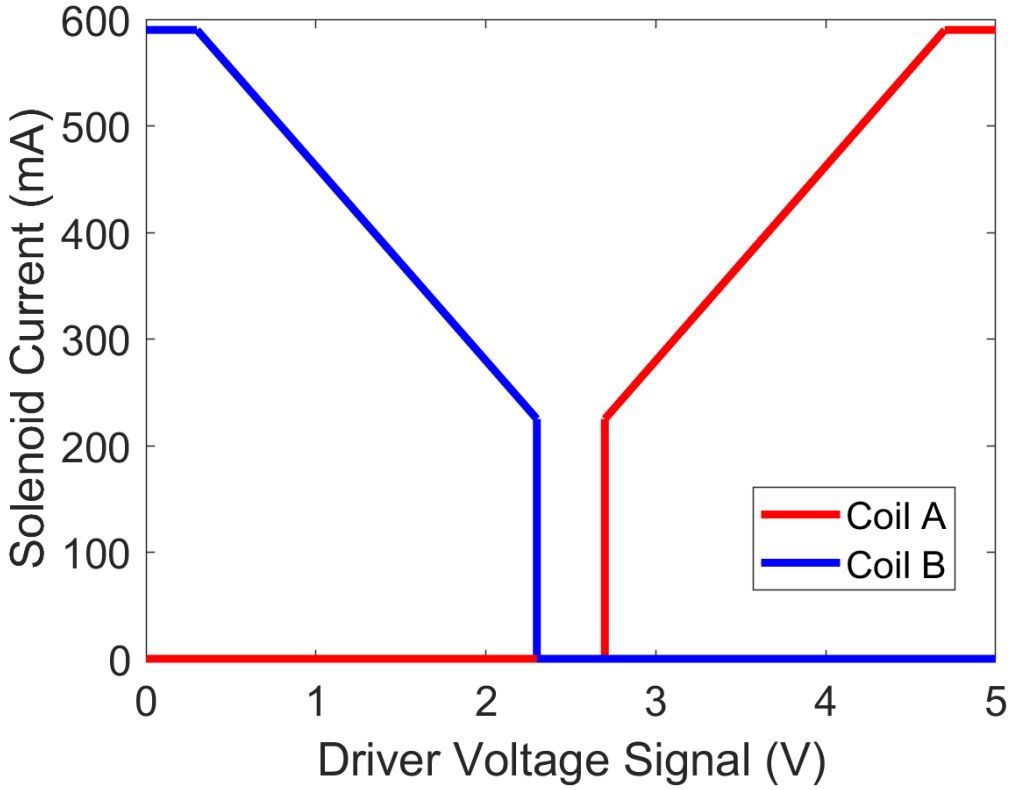

Figure H.1: Driver Signal

Appendix I

Instrumentation and Uncertainty

I.1 Sensors

The pressure, temperature, and flow sensors are part of a Flo-Tech Activa sensor array. This is a compact unit that houses the three sensors. It is located between the accumulator and the secondary pump. The flow sensor provides a 0-5 VDC output, and the pressure and temperature sensors produce a 4-20 mA signal. These sensors were previously calibrated. The sensor Array is shown in Figure I.1

The torque and speed sensors are together in a compact Futek TRS 605 sensor. This is an inline sensor that is mounted between the gearbox and secondary pump. It includes a -5-5 VDC signal output torque sensor and a TTL speed encoder. Futek performed calibration on this unit. The sensor is shown in Figure I.2.

Figure I.1: Activa Sensor Array

I.2 Uncertainty

The uncertainty of the each measurement quantifies the statistical dispersion of the measured quantity, as well as sensor specific causes for inaccuracy. The measurement uncertainty is computed by the Root-Square-Sum(RSS) of the combined DAQ uncertainty u_{DAQ}, device uncertainty u_{dev}, and statistical uncertainty u_{stat}. For the uncertainty calculation, the uncertainty was assumed to be linear with measurements.

$$u_{sensor} = \sqrt{u_{DAQ}^2 + u_{dev}^2 + u_{stat}^2} \tag{I.1}$$

The DAQ uncertainty consists of uncertainty due to accuracy, resolution, and sensitivity, which can be RSS'd to provide the overall DAQ uncertainty for each sensor. The accuracy uncertainty of the DAQ, $u_{DAQ,acc}$ depends on the full scale of the input signal,

Figure I.2: Futek TRS 605

V_{fs}. The sensitivity uncertainty of the DAQ, $u_{DAQ,sens}$ for this DAQ is less than 1% of accuracy uncertainty and is neglected in the calculation. The resolution uncertainty of the DAQ, $u_{DAQ,res}$ is also dependent on the full scale voltage and bits of resolution, n.

$$u_{DAQ} = \sqrt{u_{DAQ,acc}^2 + u_{DAQ,sens}^2 + u_{DAQ,res}^2} = \sqrt{u_{DAQ,acc}^2 + (\frac{V_{fs}}{s^n})^2 + u_{DAQ,res}^2} \quad \text{(I.2)}$$

Each sensor measurement has a specific uncertainty dependent on accuracy, precision, resolution, and sensitivity of the device, as well as other minor uncertainties, such as temperature drift, which are neglected due to having minimal effect in the test bed. The accuracy is how close to the true value can be detected, precision is the repeatability of the measurement of a signal, resolution is the smallest intervals that the sensor can pick up based on how what the sensor can resolve and output, and sensitivity is the smallest possible change that the device can detect. The total device uncertainty is

$$u_{dev} = \sqrt{u_{dev,acc}^2 + u_{dev,prec}^2 + u_{dev,sens}^2 + u_{dev,res}^2} \tag{I.3}$$

where, $u_{dev,acc}$ is uncertainty due to the device's accuracy, $u_{dev,prec}$ is uncertainty due to the device's precision, $u_{dev,sens}$ is uncertainty due to the device resolution, and $u_{dev,res}$ is uncertainty due to the sensitivity of the device. For the statistical uncertainty, 5000 data points were taken at a steady state and the data was processed with a 99% confidence level.